ACS Catalysis

Research Article

pubs.acs.org/acscatalysis

Reaction Network of Methanol Synthesis over Cu/ZnO Nanocatalysts

Luis Martínez-Suárez, Niklas Siemer, Johannes Frenzel,* and Dominik Marx

Lehrstuhl für Theoretische Chemie, Ruhr−Universität Bochum, 44780 Bochum, Germany

Supporting Information

ABSTRACT: The efficiency of industrial methanol synthesis from syngas results from a complex scenario of surface chemical reactions in the presence of dynamical morphological changes of the catalyst material in response to the chemical and physical properties of the gas phase, which are believed to explain the superior performance of the Cu/ZnO catalyst. Yet, the applied conditions of elevated temperatures and pressures substantially hamper *in situ* experimental access and, therefore, detailed understanding of the underlying reaction mechanism(s) and active site(s). Here, part of this huge space of possibilities emerging from the structural and chemical configurations of both, adsorbates and continuously altering Cu/ZnO catalyst material, is successfully explored by pure computational means. Using our molecular dynamics approach to computational heterogeneous catalysis, being based on advanced *ab initio* simulations in conjunction with thermodynamically optimized catalyst models, the resulting mapping of the underlying free energy landscape discloses an overwhelmingly rich network of parallel, competing, and reverse reaction channels. After having analyzed various pathways that directly lead from CO_2 to methanol, not only specific Cu/ZnO interface sites but also the near surface region over the catalyst surface were identified as key to some pivotal reaction steps in the global reaction network. Analysis of the mechanistic details and electronic structure along individual steps unveils three distinct mechanisms of surface chemical reactions being *all* at work, namely Eley−Rideal, Langmuir−Hinshelwood, and Mars−van Krevelen. Importantly, the former and latter mechanisms can only be realized upon including systematically the near surface region and dynamical transformations of catalyst sites, respectively, in the reaction space throughout all simulations.

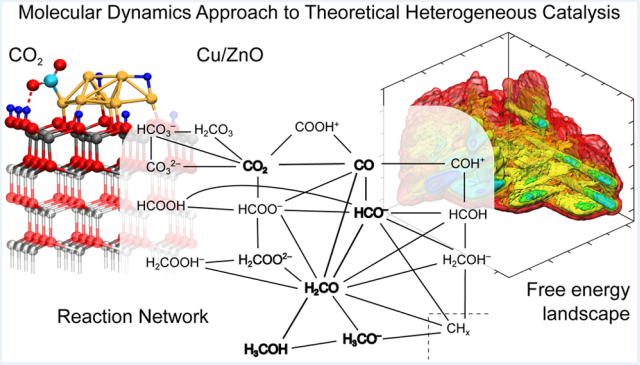

KEYWORDS: *ab initio molecular dynamics, heterogeneous catalysis, copper zinc oxide surfaces, CO_2 hydrogenation, methanol synthesis, water−gas shift, reaction mechanism, reaction network*

1. INTRODUCTION

The industrial process of methanol synthesis is of substantial technological relevance as it delivers one of the top 10 bulk chemicals[1,2] with predominant usage as feedstock for many primary derivatives and common energy carriers.[3] Nowadays, methanol is commercially synthesized, both highly selectively and most efficiently, from syngas (i.e., a mixture of H_2, CO, and CO_2), which is still generated from fossil resources but potentially might be replaced in the future by green sources such as biomass.[2] In the currently applied heterogeneous catalytic process (the so-called ICI process[4]), syngas is converted over a multicomponent material of Cu nanoparticles (between 4 and 10 nm), which are separated by ZnO with Al_2O_3 acting as a promoting component.[5−7] Upon channeling the syngas over the catalyst, both CO and CO_2 will be converted into methanol with CO_2 being the primary C_1 source when using the ICI catalyst that is based on the Cu/ZnO system.[8−12] Although thermodynamic limitations suggest the use of low temperatures, the selectivity of CO_2 hydrogenation is yet decreased by high concentrations of CO_2 in the feed gas as well as the unfavorable CO production via the reverse water−gas shift reaction.[13] Therefore, still rather harsh conditions (of temperatures and pressures of about 473−573 K and 5−10 MPa) are necessary to sufficiently accelerate the reactions and to guarantee optimal yields at highest selectivity.[1,14−16] Given the ever-expanding demands of methanol together with rising energy costs, advances in the development of more active catalysts that operate at lower temperatures and pressures in the industrial process would be most desirable.

Pivotal to catalyst improvement or even development of new catalysts in terms of rational design strategies, however, is the detailed knowledge of the structure−activity relationship in terms of knowing active site(s) and reaction mechanism(s). To resolve the physical and chemical processes on the ICI catalyst surface with atomistic resolution remains a challenging task because of the highly reactive syngas atmosphere and, in particular, the applied high pressures that severely restrict the *in situ* application of many analytic and spectroscopic experimental methods. Therefore, many studies have eluded these implications by applying much reduced pressures and/or using

Received: January 15, 2015
Revised: May 29, 2015
Published: May 29, 2015

DOI: 10.1021/acscatal.5b00442
ACS Catal. 2015, 5, 4201−4218

model catalysts. Hence, one must be careful in interpreting the results of these studies because the morphology of the nanoscopic surface structure of the Cu/ZnO system is directly coupled to the environmental conditions and composition of the gas phase.[17−25] More importantly, being immediately related to the general concept of strong-metal support interaction (SMSI),[26,27] these conditions give rise to dynamical morphological changes which might be one reason to explain the improved catalytic activity of the combined system as opposed to the individual components,[23,28−31] which themselves catalyze methanol synthesis but at significantly reduced efficiencies. Evidently, there must exist synergistic effects between the reducible ZnO and nanodispersed Cu,[22,24,25,32−34] although no consensus has been reached yet on the actual mechanism[5,6,16,18,19,21−23,28,30−32,34−58] that explains the superior performance of the ICI catalyst.[50,59] Recent experimental advances were made to disentangle structural and synergistic promotion of the combined system.[22,34] Ultimately, the activity of the catalyst also depends on the history of the reduction process.[16,23,31,45,60−63] Given all this extensive research with often conflicting results and controversial interpretation, up to now, no consensus was obtained on the active site(s) or even on the morphology of the catalyst. The coexistence of multiple effects being at work, however, suggests several active sites or even a myriad of active morphologies to be present. This is because dynamical morphological changes such as the ones induced by SMSI could even alter the performance and accessibility for some individual steps in the reaction mechanism, especially for the two hydrogenation scenarios based on CO_2 and CO in addition to the their coupling via the (reverse-) water−gas shift reaction, (r)WGSR.[61]

The role of these reactions and their contribution to the global reaction mechanism is less clear. Besides the fact that there exists no clear picture on the active site(s), the uncertainty in the mechanism also is due to the high pressures of the industrial process that limit spectroscopic *in situ* accessibility of chemical species during the process of methanol synthesis. Some effort has been made to identify C_1 species by using model catalysts often containing only one component of the ICI catalyst, using diluted reactant gases, or methanol decomposition instead, which only gave access to strongly bound or long-lived and thus stable species,[16] i.e., formate ($HCOO^-$),[64−75] carbonate (CO_3^{2-}),[67,76] and methoxide (H_3CO^-).[67,69,71]

Overcoming part of these limitations, state of the art static step-by-step computational approaches were employed to construct reaction mechanisms from well-defined static structures and interconnecting elementary reactions steps as obtained, for instance, by nudged elastic band or climbing gradient algorithms. However, in almost all studies, the complexity of the catalyst model was reduced to the Cu component, only. On the basis of the results of these computational studies, three possible reaction mechanisms are proposed over Cu catalysts (for a recent review, see ref 77): (I) formate mechanism,[6,78−85] (II) CO−hydrogenation mechanism,[84] and (III) hydrocarboxyl ($COOH^+$) mechanism.[86,87] These mechanisms mainly differ in the sequence of C−O bond breaking in the reduction process which, therefore, entail the presence of further C_1 species. Going beyond catalyst models based on low-index Cu surfaces, reaction barriers of CO_2 and CO hydrogenation are significantly lowered when computed over less simplified Zn/Cu surface alloys[6] or unsupported Cu clusters.[81] Alternatively, the shortcoming in the results of simple static kinetic modeling approaches were found to be partially improved if the morphology of $Cu/ZnO/Al_2O_3$ was taken into account.[88,89] In addition, the interaction of reactants, intermediates, and products with the catalyst surface cannot be neglected at the outset, as for instance strongly bound CO_2 blocks larger parts of the catalyst surface or may undergo exchange reactions with lattice oxygen,[11,61] whereas the role of the O adatoms present on Cu is controversially discussed.[12,16]

Notwithstanding the effects that have been demonstrated for the adsorbate interaction and Cu-free ZnO surfaces,[90−109] on Cu/ZnO catalysts C_1 species may actively contribute to sintering processes, e.g., via the formation of Cu−CO complexes which exhibit very low diffusion barriers over ZnO surfaces.[110] Thus, in the running reduction process of CO_2 and subsequently the C_1 species, the activity of the catalyst decreases due to dynamical morphological changes, which are obviously also induced by chemical interaction with (spectator) species present in the methanol synthesis process. This raises the general question if under reaction conditions there will exist only one mechanism for each of the hydrogenation reactions or if a dynamic network of many parallel and competing reaction channels will prevail over Cu/ZnO given the vast space of structural and chemical possibilities, both of chemical species and catalyst surfaces, which eventually is set by the redox conditions of the surrounding gas phase.

In this work, we have addressed the astonishingly complex puzzle of inherently coupled chemical transformations and highly dynamical materials behavior underlying the heterogeneous catalytic process of methanol synthesis from syngas by employing advanced dynamical *ab initio* simulations[111] in combination with recently developed and thermodynamically optimized $Cu_8/ZnO(000\bar{1})$ catalyst models.[24,25] We recall that discussions as to the precise nature of "the" active sites in industrial methanol synthesis are still going on, and we certainly do not claim that our computationally tractable model provides the final answer to that question. Yet, although our model is relatively small in size compared to the much more complex industrial catalysts, i.e., Cu nanoparticles with ZnO acting as a separator or support,[112−114] it describes the crucial synergistic effects as we have demonstrated in detail not long ago.[24,25] In particular, our model captures the morphology responses of the supported Cu cluster to changes in the composition and thermodynamic properties of the surrounding gas phase, as well as electronic charge transfer effects from ZnO to Cu, which has been demonstrated experimentally to enhance catalyst performance.[34,49] In stark contrast, these crucial properties of the industrially superior Cu/ZnO catalyst are not present in the less performing plain Cu catalysts, which are still used as catalyst models in much current computational work using for instance Cu surfaces or unsupported Cu clusters. Here, while keeping any *a priory* input on species and reaction mechanisms at a minimum, we show here that by pure computational means,[115,116] the highly intricate network of reaction pathways interconnecting a myriad of chemical species over Cu/ZnO can be "synthesized" *in silico* by means of accelerated finite temperature *ab initio* molecular dynamics (AIMD) sampling of a reduced but multidimensional free energy landscape. Besides having produced all relevant C_1 species discussed so far in the literature, numerous spectator species as well as adatom decorations on both the Cu nanoparticle and ZnO support were generated. This demonstrates the predictive power of our so-called "molecular dynamics approach to theoretical hetero-

DOI: 10.1021/acscatal.5b00442
ACS Catal. 2015, 5, 4201−4218

geneous catalysis"[115,116] given the much increased complexity of methanol synthesis over Cu/ZnO compared to the reaction network that we mapped previously for the bare ZnO catalyst[109,115−117] that underlies the BASF process. In the final reaction network on Cu/ZnO, the highly reactive (short living) formaldehyde species plays a central role toward the formation of the final product, methanol, out of CO_2. Moreover, the WGSR, which is present in both forward and backward directions and along different reaction pathways, was sampled in addition to water formation as well as other side reactions, such as methane synthesis over Cu and creation of oxygen vacancies via several pathways including molecular adsorbates and SMSI effects. Finally, the reduction process of the C_1 species is investigated using electronic structure analysis of selected snapshots sampled along trajectories in order to elucidate the chemical bonding aspects that underlie the genuinely dynamical processes which eventually convert CO_2 to methanol over Cu/ZnO.

2. COMPUTATIONAL METHODS

2.1. Catalyst Model and Slab Setup. The Cu/ZnO catalyst was modeled by periodic slabs consisting of 4 × 4 × 4 repeated primitive unit cells of bulk ZnO and a Cu8 nanoparticle deposited on the O-terminated ZnO(000$\bar{1}$) surface (see Figure 1). We have developed this thermodynamically optimized catalyst model only recently by an extensive exploration of the intricate stabilization mechanisms of the polar O-terminated ZnO(000$\bar{1}$) surface[99,103] with Cu[118] and linking them to the chemical and physical properties of the gas phase via a thermodynamic formalism and construction of an extended structural surface phase diagram.[24,25] This phase diagram suggested a reduced Cu_8/ZnO(000$\bar{1}$) surface phase to be present at high hydrogen partial pressures and medium oxygen partial pressures that are typically applied during industrial methanol synthesis. Similar to the Cu-free O-terminated ZnO(000$\bar{1}$) surface,[103] this thermodynamically preferred Cu/ZnO model has a coverage of 1/2 monolayer (ML) of hydrogen atoms on surface, i.e., eight hydrogen atoms per supercell with six hydrogen atoms placed on oxygen atoms and two on the copper cluster (see Figure 1). The final morphology of the copper cluster, coadsorbate decoration, and active site for the reactant molecule CO_2 were obtained via a comprehensive mapping of the potential energy surface of adsorption of CO_2 in combination with AIMD simulations and electronic structure analysis.[24,25] In all simulations, the positions of Zn and O atoms at the bottom of the slab were kept fixed at ZnO bulk positions (as depicted in Figure 1), and only the three top layers of the ZnO(000$\bar{1}$) surface, the copper cluster, adsorbate, and coadsorbate species, were allowed to move freely. Pseudohydrogen atoms of 3/2 nuclear charge were placed at the Zn-terminated bottom of the slab, which is important to guarantee charge neutrality and removal of spurious partially filled surface bands not present in bulk ZnO.[118,119] Note that without this passivation of the dangling bonds the surface slab would carry an intrinsic dipole.[118] In the supercell, the two surfaces of the slab were decoupled by a vacuum layer of ∼13 Å thicknessas measured from the topmost Cu atom.This slab system, which typically contained more than 160 atoms in total, is finally used to carry out the multidimensional *ab initio* metadynamics simulations in order to explore the free energy landscape that governs the hydrogenation of CO_2 to yield CH_3OH on Cu/ZnO.

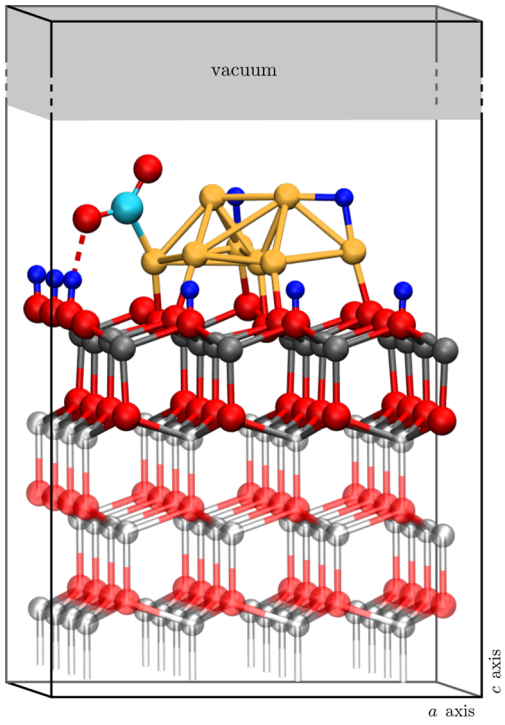

Figure 1. Schematic view of the thermodynamically optimized[24,116] nanocatalyst slab model: The ZnO(000$\bar{1}$) surface, being covered by a total of 1/2 ML hydrogen and supporting a Cu_8 cluster. The nanocatalyst model is in a reduced oxidation state with an activated reactant CO_2 molecule being adsorbed on the Cu cluster. This structure[24] is used to start our 3D metadynamics simulations (see text). Gray is used for zinc, red for oxygen, orange for copper, cyan for carbon, and blue for hydrogen. Atomic positions of the bottom layers of ZnO (light faded color) were kept fixed during the AIMD simulations.

Before moving on, we pause for a moment to refer to the relevance of such a rather small cluster/support model to decipher the reaction mechanisms that underlie large-scale catalytic processes used in industry. It is acknowledged that not only is the cluster size far from the size range of copper particles in the ICI catalyst but a small periodic surface slab cannot represent the structurally ill-defined binary ZnO/Al_2O_3 support material that is used in the industrial process. However, we like to refer to the careful discussion of the expected Cu cluster size effects on the surface phase diagram[24,25] underlying our Cu/ZnO catalyst model as provided in the Supporting Information of ref 24. It has been demontrated therein that the presently used cluster model already captures the qualitative features of the surface phase diagram, subject to shifts of phase boundaries, compared to larger clusters (see pp 4−6). Moreover, using deposited cluster models consisting of on the order of 10 metal atoms is commonplace in state-of-the-art computational catalysis studies[120−125] in which chemical interactions and reactions are studied based on nonsemiempirical electronic structure methods (it is noted that these studies are mostly carried out in the static optimization limit, whereas we carry out full *ab initio* simulations at finite temperature in the present investigation). Most importantly, studying heterogeneous catalysis in the limit of small, size-selected clusters is by now a well-established and useful contribution to understanding the related industrial processes.[126−132] We therefore conclude that the results extracted from the current catalyst model will lead to valuable contributions toward better understanding the

DOI: 10.1021/acscatal.5b00442
ACS Catal. 2015, 5, 4201−4218

molecular reaction mechanism of methanol synthesis from CO_2 on Cu/ZnO catalysts.

2.2. Electronic Structure. The electronic structure was calculated using Kohn−Sham density-functional theory (DFT). We used the gradient-corrected exchange-correlation functional by Perdew, Burke, and Ernzerhof.[133,134] The core electrons were described by Vanderbilt's ultrasoft pseudopotentials.[135] Zinc *3d* electrons were treated explicitly in these electronic structure calculations. At virtually no loss in accuracy in the AIMD simulations for those Zn atoms located in the two layers of zinc at the bottom of the slab, these electrons were included in the pseudopotentials. A plane wave basis was employed in all calculations including plane waves up to a kinetic energy cutoff of 25 Ry, which gives well converged results for bulk ZnO.[118,119] Single-point electronic band structure and density of states (DOS) calculations were carried out with the PWscf code of the Quantum−Espresso package.[136] A 2 × 2 × 1 Monkhorst−Pack *k*-point mesh[137] was used for calculation of the self-consistent electronic density. Atom- and state-resolved DOSs were obtained by projection of the electronic density on an atomic-centered basis set.[138] This type of approach has been demonstrated previously to yield consistent results for charge transfer when compared to real-space methods based on Bader analysis and also Mullikan charges for a closely related metal/oxide system, namely Au_n/TiO_2 interacting with water, which is a catalyst for mild methanol oxidation directly with O_2.[139] The resulting electronic populations q_i of atoms of type i of a AIMD snapshot were used to calculate the electronic charge transfer $\Delta q_i = q_i - q_i^{ref}$ with respect to q_i^{ref} of a reference of two isolated systems, i.e., a free CO_2 molecule and the 1/2−H−sym-Cu_8/ZnO(000$\bar{1}$) surface model as a reference. Dispersion forces were included using the empirical approach of Grimme.[140] Note that this setup of the electronic structure calculations is identical to the one used in our recent studies[24,25] in which we have demonstrated in detail the accuracy of the methods employed for the present purpose. In addition, for a similar system, namely Au_n/TiO_2 being relevant to methanol oxidation, the size and shape dependence of the metal cluster was studied with no appreciable effect found upon varying the number of noble metal atoms in the size range of roughly 10 to 20 atoms.[141]

2.3. Free Energy Sampling. All AIMD simulations were performed within the Car−Parrinello[142] propagation scheme[111] and have been carried out using the CPMD software package.[143] The canonical (NVT) ensemble was established at a temperature of 500 K using Nosé−Hoover chains[144] to thermostat both the ions and the orbital degrees of freedom. In the case of the ions, one independent Nosé−Hoover chain has been coupled to each of the Cartesian coordinates of all mobile ions (called "massive thermostatting") in order to most efficiently generate the canonical ensemble. A fictitious mass of 700 a.u. for the electrons was sufficient to decouple their dynamics CP adiabatically[111] from the one of the ions. The mass of deuterium was used for hydrogen ions to allow for a larger AIMD time step of Δt = 6 a.u. (≈ 0.145 fs). The electronic structure for the AIMD simulations was calculated using the Γ point only.

Ab initio metadynamics sampling,[145] see, *e.g.*, refs 111 and ref 146 for recent reviews, was used to compute the multidimensional free energy surfaces (FES) that underlie these surface chemical reactions. Stability and efficiency of the CP sampling was preserved by using the extended Lagrangian formulation of metadynamics.[147] Multidimensional reaction coordinates as spanned by three generalized collective variables (CV) were employed to sample the FES. As CVs we used coordination numbers c[C−O], c[C−H], and c[O−H] according to

$$c[X-Y] = \sum_{ij} \frac{1-(d_{X_iY_j}/d^0_{XY})^p}{1-(d_{X_iY_j}/d^0_{XY})^{p+q}} \quad (1)$$

with the interatomic distance $d_{X_iY_j}$ calculated between atom X_i and atom Y_j out of selected sets of atoms $\{X_i\}$ and $\{Y_j\}$ using cutoff parameters d^0_{XY} of d^0_{CO} = 1.35 Å, d^0_{CH} = 1.20 Å, and d^0_{OH} = 1.20 Å. The exponents p and q were set to 16/6, 24/4, and 24/4 for c[C−O], c[C−H], and c[O−H], respectively. Herein, c[C−O] described the bond breaking as well as the creation of bonds between the carbon atom and the two oxygen atoms of CO_2 as well as oxygen atoms building up the ZnO(000$\bar{1}$) surface. The interaction of the carbon atom and the oxygen atoms of CO_2 (as defined in the reactant state) with all hydrogen atoms in the system was mapped by c[C−H] and c[O−H], respectively.

Along the AIMD-generated dynamics of the CVs, Gaussian type functions of constant height ω = 2.0 k_BT_{500} (≈0.086 eV) and constant width Δs = 0.05 were dropped building up the non-Markovian biasing potential of our metadynamics simulation. The accumulated total biasing potential provides at the end of a metadynamics simulation a direct estimate of the FES within the selected CV space.[145,148] After an initial period with a rough filling of most of the free energy minima (FEM), the simulations were continued with smaller Gaussian hills of ω = 2/3 k_BT_{500} to generate a refined FES. Following ref 149, in both setups new hills were added after 16 AIMD timesteps but not before a minimum displacement of the CV coordinate by 1.5 Δs with respect to the position of the last added hill has occurred. Effective filling of the anisotropic free energy wells was ensured by applying scaling factors $w_{c[C-O]}$ = 1.0, $w_{c[C-H]}$ = 0.8, and $w_{c[O-H]}$ = 0.8. In ref 150, it was shown that in the limit of sufficient sampling the added potential along the metadynamics trajectory corresponds to the FES spanned by the CVs subspace. The multiple walker technique of metadynamics[148,151] with up to 10 coupled replica of the AIMD system was employed to port the simulation efficiently to supercomputer resources. Before initiating the metadynamics samplings, the reactant states were equilibrated in the NVT ensemble for more than 6 ps of AIMD simulation. We have performed two metadynamics simulations. The more extensive one started from CO_2 (see Figure 1) and accumulated in total 1.8 ns of underlying AIMD simulation time, and a shorter one started from formaldehyde that replaced CO_2 in the reactant state. In the following discussion, we always refer to the metadynamics run starting from CO_2 being the reactant species, if not stated otherwise.

3. RESULTS AND DISCUSSION

Let us start the discussion of the reaction network of methanol synthesis from CO_2 over the Cu_8/ZnO(000$\bar{1}$) catalyst by using the slab model shown in Figure 1, which has a Cu_8 nanocluster deposited on a (4 × 4) supercell of the polar O-terminated ZnO(000$\bar{1}$) surface (see section 2.1). As a result of computing the thermodynamic surface phase diagram, we have obtained this optimized catalyst model only recently.[24] It belongs to the surface phase with label 1/2−H, which is the phase that is relevant to those physical and chemical conditions as being applied for industrial methanol synthesis, i.e., high hydrogen

DOI: 10.1021/acscatal.5b00442
ACS Catal. 2015, 5, 4201−4218

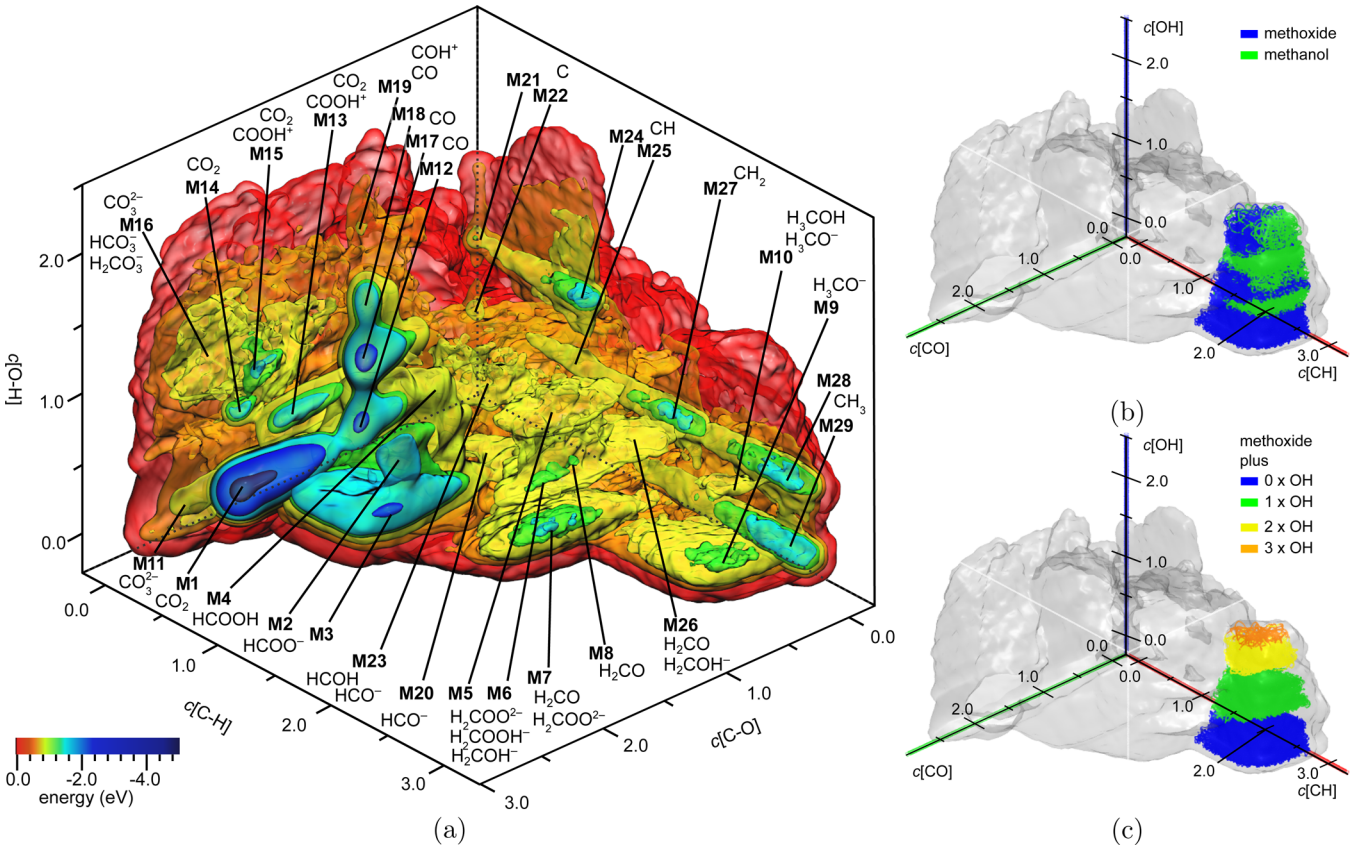

Figure 2. Free energy landscape from the metadynamics sampling of methanol synthesis based on CO_2 over the reduced $Cu_8/ZnO(000\bar{1})$ catalyst surface model (a). The coordination numbers c[C−O], c[C−H], and c[O−H] (see text) were employed as collective variables (CVs) to describe the interaction of the carbon atom with the oxygen atoms of the top layer of ZnO and the two oxygen atoms of the reactant CO_2, the carbon atom with all hydrogen atoms in the system, and all hydrogen atoms with the two oxygen atoms of the reactant CO_2, respectively. Relative free energies ΔF are reported according to the shown color scale. Bold capital **M** plus a number labels distinct free energy minima. The reported chemical formulas of C_1 species, generated over the catalyst surface at each meta time step, were obtained from analyzing the AIMD trajectory underlying the metadynamics sampling in terms of structural motifs (see text). Based on this analysis, subfigure b maps the overlapping distributions of the two C_1 species "methoxide" and "methanol" on the free energy landscape (see text). Subfigure c shows the distribution of one of these species in CV space, namely methoxide, that is subdivided with respect to the number of O−H bonds of C_1-species and adspecies (included in CV c[O−H], such as oxygen atoms, water molecules, and hydroxyl groups) that are either found on the Cu_8 cluster or located in the near surface region over the catalyst surface. The full analyses of the evolution of C_1 species as well as coadsorbate species on the free energy landscape are shown in Figures S1 and S2 in the Supporting Information, respectively.

partial pressure and medium oxygen partial pressure.[24] Exposed to such extreme conditions of the gas phase, the catalyst model is in a reduced oxidation state which allows the activation of CO_2 over Cu_8 (see Figure 1 and ref 24). In this process, the Cu_8 cluster receives electronic excess charge from the ZnO surface conduction band which was occupied by a surplus of electrons stemming from hydrogen adsorbed at oxygen dangling bonds of $ZnO(000\bar{1})$.[24,25] Indeed, such electronic charge transfer from high-lying ZnO states to the copper Fermi level was observed recently by electron paramagnetic resonance spectroscopy.[34,49] For the reduction process of the reactant, CO_2, our reduced $Cu_8/ZnO(000\bar{1})$ catalyst model has four excess electrons available in total. Besides two electrons from the ZnO conduction band the remaining two come readily with the two hydrogens bound to the Cu_8 cluster (see Figure 1).[24,25] In this setup, the catalyst model would allow reduction of the C_1 species to the oxidation state of formaldehyde, *e.g.*, via

$$CO_2 + 2e^- \rightarrow CO + O^{2-} \quad (2)$$

$$CO + 2H \rightarrow H_2CO \quad (3)$$

Obviously, each reduction step of the C_1 species involves an oxidation of the catalyst surface. For example, after reaction eqs 2 and 3, our catalyst model remains in a fully oxidized state because it provided four electrons and two protons to the generated product species, H_2CO. The catalyst surface needs to be rereduced, *e.g.*, by hydrogen adsorption from the gas phase, as defined by the applied thermodynamic conditions of methanol synthesis. Now the full reduction to methanol can be accomplished, *e.g.*, via

$$H_2CO + 2H^+ + 2e^- \rightarrow H_3COH \quad (4)$$

In the industrial process, this can occur at any time in the catalytic cycle, whereas it is not part of our metadynamics simulation.

The chemical processes involved in this type of surface reactions possess high activation barriers which on the AIMD time scale are rare events and, therefore, unaccessible using unbiased time evolution. In order to be sampled, these reactions need to be accelerated using enhanced sampling techniques. For the complete transformation of CO_2 into methanol, this comprises at minimum four hydrogen transfer

DOI: 10.1021/acscatal.5b00442
ACS Catal. 2015, 5, 4201−4218

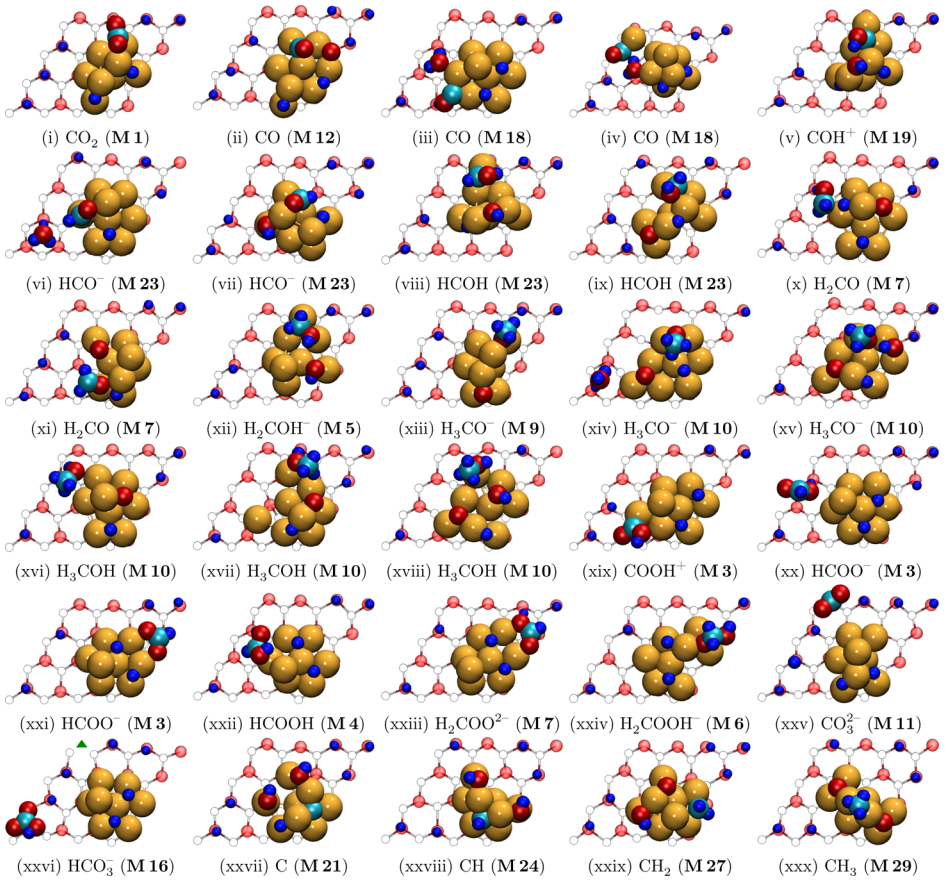

Figure 3. Representative snapshots of C_1 species over the $Cu_8/ZnO(000\bar{1})$ nanocatalyst model taken from the *ab initio* molecular dynamics trajectory underlying the metadynamics sampling of the free energy landscape (see Figure 2a). The subfigure captions identify the C_1 species by their chemical formula and the approximate location of the snapshot structure on that free energy landscape is encoded by the **M** label (in parentheses) of the corresponding free energy minimum. Ordering of the subfigures starts with the reactant state of the metadynamics simulations (compare also to Figure 1), then continues with respect to increasing number of C−O and C−H bonds, and ends with the CH_x species. The nomenclature of the species was chosen according to stable gas phase species and does not impose a particular charge state.[109,115,117] Only the first ZnO bilayer of the surface is shown for clarity, but the extended slab shown in Figure 1 was used throughout the metadynamics simulations. Atoms of the copper nanoparticle, C_1 species, and coadsorbate species adsorbed on Cu_8 as well as species that have been desorbed transiently into the near surface region over the catalyst are highlighted by larger spheres to guide the eye. Small green triangular symbols mark oxygen vacancies present on the $ZnO(000\bar{1})$ surface for structures xiv, xv, xviii, and xxvi. Except for the last subfigure, the vacancy is located at the Cu/ZnO interface and therefore mostly hidden to the eye. The same color scheme as in Figure 1 was used to distinguish the different elements involved.

reactions and the abstraction of one oxygen atom from the C_1 species corresponding to the reactions according to eqs 2, 3, and 4. In view of exploring all possible pathways and species of the whole reaction network, we have decided to accelerate the coordination (and thus covalent bonding) between carbon and oxygen, carbon and hydrogen, and oxygen and hydrogen; i.e., we sample the subspace spanned by the three CVs c[C−O], c[C−H], and c[O−H] as introduced in section 2.3. Choosing this set of CVs, we leave a maximum of flexibility to the system as we do not enforce or impose any pathway or chemical species by *a priori* input. Hence, our set is general enough to even allow the exploration of side reactions, i.e., rWGSR and WGSR as well as methanation or coking of the catalyst.

Exchange reactions between surface and gas phase reactions are particularly important as they allow the transport of molecular species between ZnO and Cu (active) sites. These processes of desorption and readsorption of products and reactants encompass a large configuration space. In our metadynamics setup tailored to explore the reaction network of methanol synthesis over Cu/ZnO, these degrees of freedom will be sampled by standard AIMD which implicitly includes them to the global three-dimensional FES. It is stressed that with this metadynamics setup we aim to explore the reaction network of methanol synthesis from CO_2; i.e., we use this procedure to identify all possible types of C_1 species and reaction channels present over $Cu_8/ZnO(000\bar{1})$, but neither intended the converged calculation of an accurate FES nor of free energy barriers. Such a refinement can be accomplished most efficiently in subsequent computations using dimensionally restricted sampling setups, for instance based on thermodynamic integration (via "blue moon" sampling[111]), that are specifically tailored to individual reaction channels or elementary reaction steps that are suggested by the present global exploration.[116]

The FES obtained from the metadynamics sampling of three CVs and starting from CO_2 is depicted in Figure 2a. It features a multitude of free energy minima (FEM) which are labeled **M1** through **M29** which are characterized by coordinates in CV space as summarized in Table S1 in the Supporting Information. In addition, Figure 2a and Table S1 list all types of C_1 species which were sampled *within* a distinct free energy minimum on this three-dimensional FES. These species were

DOI: 10.1021/acscatal.5b00442
ACS Catal. 2015, 5, 4201−4218

extracted from the AIMD trajectory underlying the metadynamics simulation by analysis of each and every meta time step (for details see section 2 in the Supporting Information). Representative snapshots of these C_1 species over the catalyst surface are depicted in Figure 3. We note in passing that these snapshots do not necessarily represent atomistic structures at the minimum of the FEMs as the listing of Figure 2a or Table S1 in the Supporting Information may suggest at a first glance.

The AIMD trajectory that underlies metadynamics sampling of the free energetics of the processes moreover provides the basis for a classification of the elementary chemical reactions over the $Cu_8/ZnO(000\bar{1})$ catalyst model which give rise to a complex network with several interwoven and crossing pathways (see Figure 4). In addition to C_1 species, with

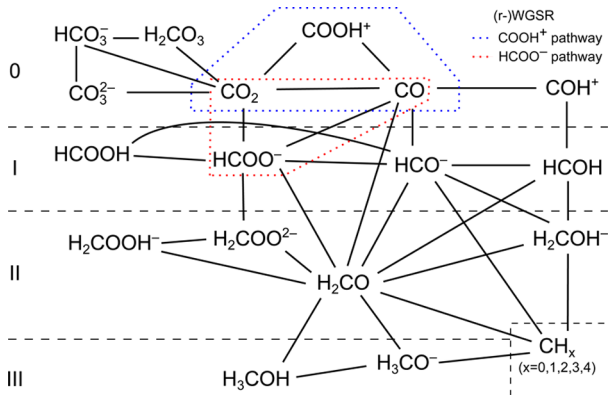

Figure 4. Schematic reaction network of methanol synthesis from CO_2 on the present $Cu_8/ZnO(000\bar{1})$ nanocatalyst model (see Figure 1) as obtained by pure computational means via *ab initio* metadynamics mapping of the free energy landscape. The chemical formula and formal charge state of the various C_1 species was chosen according to the corresponding stable gas phase species. Solid black lines represent elementary chemical reaction steps between these species, i.e., hydrogen transfer reactions, oxygen transfer, electron transfer, as well as combinations of these processes that have been generated by simulation. Species involved in different mechanisms of the (reverse-) water−gas shift reaction ((r-)WGSR) are indicated by colored dotted frames. Roman numbers on the left indicate the number of H atoms bound to the carbon atom. Note that the initially reduced $Cu_8/ZnO(000\bar{1})$ catalyst model becomes successively oxidized as CO_2 gets reduced (from top to bottom in this scheme) to yield H_3COH.

pathways directly leading from CO_2 to the desired product methanol (see Figure 3i−xviii in addition to Table 1), this network comprises prominent side reactions. These are well-known for the Cu/ZnO catalyst, i.e., (r)WGSR as well as carbonation, coking, and methanation (see Figure 3i−iv and v as well as xxv through xxx). Furthermore, along with reduction of CO_2, noncarbon containing coadsorbate species such as O adatoms, OH groups, and H_2O molecules were observed to be formed on the Cu_8 cluster (see Figure 3iii−xviii and xxvii−xxx and Table 1 for a detailed analysis of the resulting coadsorbate decoration). During metadynamics simulations, these coadsorbate species were formed by (i) dissociation of one O atom of the initial reactant CO_2 or (ii) creation of an O vacancy (O_{vac}) on the ZnO surface and (iii) successive hydrogen transfer reactions to these two types of O atoms. The formation of coadsorbate species with O−H bonds can result in overlapping distributions of two or more C_1 species when mapped onto the FES (see Figure 2b for methoxide and methanol and Figure S1 in the Supporting Information for other species) since they lead to similar or even identical CV values. The reason is that both types of OH groups, i.e., those bound to the carbon atom and OH coadsorbate species, were accelerated jointly via $c[O-H]$. By extending the analysis of the AIMD trajectory, contributions of coadsorbate species and C_1 species to the FES were disentangled, *e.g.*, methoxide and in the presence of OH adspecies (see Figure 2c). The corresponding mapping of all other C_1 species is summarized in Figure S2 in the Supporting Information. We note in passing that, in principle, full unfolding of this FES in terms of all individual reactive species (such as those partially analyzed *e.g.*, in subfigure b) combined with the specific state of the catalyst in terms of adspecies (*e.g.*, those disentangled in subfigure c) and "oxidation state landscape" (see Figure 5 in ref 25) would provide access to all associated free energies. However, there are already about 35 species involved which, in combination with the catalyst, would lead to an overwhelmingly high-dimensional reactive subspace which currently is beyond practical access for reactive surface chemical systems of the required compexity.

What is particularly important for the chemical dynamics is that our metadynamics sampling explored a multitude of different adsorption sites and thus potential active sites on all components of the catalyst model, i.e., Cu, ZnO, and the Cu/ZnO interface. During the sampling procedure, these different sites and thus possible reaction pathways were connected by species that were found to desorb transiently into the near surface region over the $Cu_8/ZnO(000\bar{1})$ surface with subsequent readsorption. Table 1 summarizes all these sites while also listing different coadsorbate species combinations sampled throughout the metadynamics simulation. By providing this information, Table 1 gathers the overwhelming structural variety and change in the surface morphology of $Cu_8/ZnO(000\bar{1})$ during the reduction of the C_1 species plus those present at side reactions.

In the following subsections, we will discuss all these aspects underlying the reaction network of Figure 4 in more detail. We have structured our discussion along the increasing degree of hydrogenation at the C_1 atom, i.e., starting from CO_2 and ending with methanol and methoxide. In addition to addressing side reactions and changes in the redox state of the $Cu_8/ZnO(000\bar{1})$ catalyst model along the CO_2 reduction, we conclude with a comparison of our reaction network to several pathways that have been previously proposed for methanol synthesis from CO_2 over ideal copper surfaces.

3.1. From CO_2 to Species with One C−H Bond Including the (r)WGSR Processes. Starting from activated CO_2 on Cu_8 (see Figure 3i), our metadynamics simulation explored different reactions directly at this site of the catalyst. $HCOO^-$ is found to be formed from one of the preadsorbed hydrogen atoms which hydrogenates the C atom of CO_2. A direct decomposition pathway of $HCOO^-$ adsorbed on top of the Cu_8 cluster yields HCO^- and an O adatom. Alternative pathways of $HCOO^-$ formation were sampled over the partially hydroxylated O-terminated $ZnO(000\bar{1})$ surface. Herein, surface hydroxyl groups provide H^+_{surf} species which react with the C atom of physisorbed CO_2 (see Figure 3xx). ZnO as a reaction site became accessible to the C_1 species after desorption into the near surface region over $Cu_8/ZnO(000\bar{1})$ and readsorption on a Cu-free part of the catalyst surface. Including the relocation of this C_1 species back to Cu, such transfer reactions between both catalyst components were extensively generated along our metadynamics simulation. Alternatively, physisorp-

DOI: 10.1021/acscatal.5b00442
ACS Catal. 2015, 5, 4201−4218

Table 1. Structural Variability As Well As Adsorbate and Adatom Decoration of the $Cu_8/ZnO(000\bar{1})$ Catalyst Surface Model in the Presence of the C_1 Species As Generated by the *ab Initio* Metadynamics Sampling of Methanol Synthesis from CO_2[a]

				no. of atoms/vacancies bound/present					
				$ZnO(000\bar{1})$			Cu_8		
C_1 species	C_1 species location on $Cu_8/ZnO(000\bar{1})$	structure example (AIMD snapshot)	$Cu_8/ZnO(000\bar{1})$ surface phase label	Cu	H	O_{vac}	H	O	OH
CO_2	Cu	Figure 1	1/2−H	5	6	0	2	0	0
CO	Cu, near surface	Figure 3iii,ii,iv	3/8−H, 1/2−H	7	5	0	2	0	0, 1
COH^+	Cu	Figure 3v	3/8−H+OH	6	4	0	2	0	1
HCO^-	Cu	Figure 3vi,vii	5/16−H, 3/8−H+OH	5−7	4, 5	0	1, 2	0, 1	0, 1
HCOH	Cu	Figure 3viii,ix	5/16−H, 3/8 H+OH	6	4, 5	0	1	0, 1	0, 1
H_2CO	Cu, phys, near surface	Figure 3x	3/8−H+O	6, 7	3−5	0, 1	0−2	0, 1	0−2
H_2COH^-	Cu	Figure 3xii	1/4−H+OH	6	4, 5	0	0	0, 1	0, 1
H_3CO^-	Cu, phys	Figure 3xiii	5/16−H+O	5−8	3, 5	0, 1	0−2	0−2	0, 1
H_3COH	phys, Cu	Figure 3xvii,xviii	1/4−H+O, 3/16 H+O+OH	6, 7	3	0, 1	1	1, 2	0
CO_2	Cu, near surface	Figure 3i	1/2−H	5−7	4−6	0, 1	2	0	0, 1
$COOH^+$	Cu	Figure 3xix	7/16−H	6, 7	5	0	2	0	0
$HCOO^-$	Cu, phys, ZnO	Figure 3xx,xxi	7/16−H, 3/8−H	6, 7	4, 5	0, 1	1, 2	0	0
HCOOH	Cu, phys	Figure 3xxii	3/8−H	7	4	0	2	0	0
H_2COO^{2-}	Cu, ZnO	Figure 3xxiii	3/8−H	5−8	3−5	0	0−2	0, 1	0, 1
H_2COOH^-	Cu, ZnO	Figure 3xxiv	5/16−H	5−7	3, 4	0	0, 2	0, 1	0, 1
CO_3^{2-}	Cu, ZnO	Figure 3xxv	1/2−H	5−7	4−6	1	0, 2	0−2	0, 1
HCO_3^-	Cu, ZnO, phys	Figure 3xxvi	7/16−H+O_{vac}	5−7	4, 5	1	2	0	0, 1
H_2CO_3	Cu, ZnO, phys		3/8−H+O_{vac}	6−7	4	1	2	0	0
C	Cu	Figure 3xxvii	3/8−H+1/8−OH, 3/8−H+O+OH	6	5, 6	0	0, 1	0−2	0−2
CH	Cu	Figure 3xxviii	5/16−H+1/8−OH	5, 6	5	0	0, 1	0−2	0−2
CH_2	Cu	Figure 3xxix	5/16−H+OH+O	6	4, 5	0	0, 1	1, 2	0, 1
CH_3	Cu	Figure 3xxx	5/16−H+1/8−O	6	4, 5	0	0	1, 2	0, 1
CH_4	Cu, near surface		3/8−H+O	6−8	4	0	2,3	1	0

[a]The corresponding location and type of interaction of the C_1 species is specified in the second column using the labels "Cu," "ZnO," "phys," and "near surface" to denote chemisorbed species on Cu_8, chemisorbed on $ZnO(000\bar{1})$, physisorbed species, and species located in the near surface region over the catalyst surface, respectively. The next two columns establish the links to the selected snapshots of representative (adsorbate) C_1 atomic structures in Figures 1 and 3 and to the corresponding $Cu_8/ZnO(000\bar{1})$ surface phases, respectively, which are labeled following the nomenclature introduced together with the thermodynamic surface structural phase diagram (see refs 24, 25; the surface phase label encodes the following information: First, the coverage of the catalyst surface by hydrogen is given w.r.t. fractions of a monolayer. If present on the copper nanoparticle, an optional plus sign adds a chemical formula of co-adsorbates, *i.e.,* O, OH, as well as "O_{vac}" which denotes the presence of an O vacancy on the ZnO surface of the slab model). The six columns to the right list the (varying) number of directly adjacent atoms and oxygen vacancies present on ZnO and Cu_8 surfaces of the catalyst model as explored during the complete metadynamics simulation. Reactant species CO_2 on the thermodynamically optimized catalyst model was used as the initial reactant state for metadynamics sampling (see Figure 1). CH_4 species were obtained from preliminary two-dimensional *ab initio* metadynamics simulations (see section 3.4).

tion plus migration pathways of C_1 species over the hydroxylated $ZnO(000\bar{1})$ were accelerated via c[O−H]. For $HCOO^-$, these migration pathways were explored comprehensively including the relocation to the Cu_8 cluster (see Figure 3xx and xxi). Being adsorbed with the C atom to a Cu atom at the Cu/ZnO interface, such $HCOO^-$ species gave HCOOH after reaction with H^+_{surf} species from ZnO (see Figure 3xxii). In this configuration, HCOOH was found to decompose back via the reverse pathway. A new reaction channel for $HCOO^-$ opened up only when this species was bound with one O atom to a Cu atom at the Cu/ZnO interface. In such configurations, the other O atom of $HCOO^-$ successively receives two H^+_{surf} species from ZnO with HCOOH being a possible intermediate before C−O bond breaking and H_2O formation. The generated HCO^- species undergoes subsequent decomposition to CO and a new H^+_{surf} binding to a bare O atom of the $ZnO(000\bar{1})$ surface (see Figure 3iii). Taken together, the latter reactions constitute a reaction channel of the rWGSR, which takes place at the $Cu_8/ZnO(000\bar{1})$ interface and via the $HCOO^-$ species. Similarly, on Cu_8 the direct decomposition of $HCOO^-$ was sampled via two pathways giving (i) HCO^- and an O adatom as well as (ii) CO and a OH adspecies.

Besides pathways involving $HCOO^-$ species, the metadynamics sampling explored also the rWGSR channel via $COOH^+$ species, which is considered to act as the main intermediate in both WGSR and rWGSR processes over low-index Cu surfaces and isolated Cu nanoparticles.[81,82,152] Over our catalyst model, $COOH^+$ is formed from CO_2 being adsorbed with the C atom at the metal part of the Cu/ZnO interface together with a H^+_{surf} species taken from the ZnO component (see Figure 3xix). Given this configuration, the $COOH^+$ species dissociate into CO and a OH^- coadsorbate species, which becomes protonated to H_2O by adjacent H^+_{surf} OH groups of ZnO (see Figure 3iii). Note that in this part of the reaction network the two H adatoms do not react with C_1 species although the corresponding degrees of freedom were explicitly sampled by our metadynamics setup. These observations suggest that the availability of OH groups, i.e., H^+_{surf} species, directly at the Cu/ZnO interface are highly important to facilitate the rWGSR. The role of these surface OH groups may be similar to the one of H_2O on Cu(111), at which CO_2 conversion to $COOH^+$ via transfer of one hydrogen atom from a neighboring H_2O molecule is preferred over transfer of one H atom adsorbed on Cu.[86,87] More importantly, recent experimental studies on

DOI: 10.1021/acscatal.5b00442
ACS Catal. 2015, 5, 4201−4218

oxide-supported metal nanoparticles, *e.g.*, Cu/ZnO among others, demonstrated the important role of the support material in activating the catalyst toward WGSR and, thus, significantly increasing the activity with respect to low-index metal surfaces or unsupported metal nanoparticles.[153,154]

For CO species, three reaction pathways were sampled which all exclusively proceed over Cu_8 with the reactants being preadsorbed there. The first pathway leads to CO_2 via the reaction of CO and an adjacent O adatom (see Figure 3ii). On the one hand, the sampling of this pathway, which is part of the WGSR, may resemble only the simple back-reaction to the initial reactant state of the metadynamics simulation. On the other hand, it discloses an open pathway to effectively remove O adspecies from Cu_8 by CO stemming from syngas via CO_2 production and subsequent desorption. Thus, alongside the alternative channel via H_2O formation, this pathway from CO could prevent full coverage of the Cu nanoparticle by OH and O coadsorbate species, respectively, which are continuously evolving as side products from mandatory C−O bond cleavage reactions of CO_2 toward methanol. For the industrial process, such deoxygenation reactions might explain the promoting role of CO in the feed gas of methanol synthesis, which is believed to maintain the catalyst in an active state.[16] In addition, only very recently H_2O cofeeding experiments provided strong evidence for a mechanistic promotion of CO_2 hydrogenation by the WGSR process.[23] A direct participation of H_2O in reactions on the Cu cluster was sampled by metadynamics. Besides H adatoms on Cu, a H_2O molecule was one possible reaction partner in the second type of pathway leading from CO to COH^+ species, i.e., (i) via the protonation by an adjacent H of a coadsorbed H_2O and (ii) via transfer of a H adatom on Cu to CO (see Figure 3v). In the third pathway explored by the metadynamics sampling, CO reacts with a H adatom of the Cu_8 cluster to give HCO^- (see Figure 3iii and vi, respectively). Finally, reaction pathways of HCO^- and COH^+ are found to lead to HCOH species over Cu_8 via hydrogen transfer reactions at the O atom and C atom, respectively (see Figure 3viii and ix).

3.2. The Key Intermediate H_2CO and Other Species with Two C−H Bonds. In the reaction network of Figure 4, the highly reactive H_2CO species takes over a central role. Six reaction pathways leading to this species were sampled by the 3D metadynamics simulation. Starting from $HCOO^-$, it underwent C−O bond scission and hydrogen transfer reactions which, besides via the direct way, was achieved also via the formation of H_2COO^{2-} and H_2COOH^- species. Alternatively, hydrogen transfer reactions were sufficient when the reactants were HCO^-, HCOH, and H_2COH^-. Once synthesized, the H_2CO species either remain adsorbed or desorb into the near surface region over the $Cu_8/ZnO(000\bar{1})$ surface.

A HCO^- species prior to its reaction with a neighboring H adatom to give H_2CO according to the first pathway is depicted in Figure 3vii. An alternative pathway was also sampled in which HCO^- abstracts the H atom from a OH adspecies on Cu_8 to give H_2CO, thus leaving an O adatom behind. In the second pathway, the species HCOH (see Figure 3ix) undergoes an intramolecular rearrangement in which the hydrogen is transferred from the O atom to the C atom of the C_1 species. Closely related to this observation is the fact that this reaction was shown to be exothermic both in the gas phase and over the polar Zn-terminated ZnO(0001) surface and, therefore, was suggested to be a reaction step in methanol synthesis from CO.[155] In our reaction network, the third pathway to H_2CO is characterized by a H_2COH^- species in the reactant state. This species decomposes over Cu_8 and leaves an H adatom behind. Over the Cu_8 cluster, the H_2COH^- species themselves were formed (i) from HCOH reacting with an H adatom (see Figure 3xii) and (ii) from HCO^- via the concerted hydrogen transfer reaction of two H adatoms. For the H_2COH^- species, there exists a putative reaction pathway directly to the desired product methanol by only one further hydrogen transfer reaction. However, such a reaction channel seems to be closed as it was not sampled over $Cu_8/ZnO(000\bar{1})$ and, therefore, suggests H_2COH^- to act merely as a spectator species in the reaction network. Only very recently, a similar result was reported for the related process of methanol synthesis from CO over reduced $ZnO(000\bar{1})$ surfaces over which the decomposition of H_2COH^- species into H_2CO species was kinetically preferred on the FES rather than the subsequent conversion to H_3COH.[116,117]

The remaining three pathways from $HCOO^-$, H_2COO^-, and H_2COOH^- to H_2CO all involve the crucial dissociation reaction of one of the two C−O bonds. Here, the simplest scenario is an abstraction reaction in the case of the H_2COO^{2-} species. Indeed, the metadynamics simulations sampled this reaction over Cu_8 leading to an O adatom as coadsorbate species in the product state. The H_2COO^{2-} species itself was formed from $HCOO^-$ via a pathway involving the Cu/ZnO interface; Figure 3xxi shows $HCOO^-$ which is adsorbed with both O atoms at Cu_8. In such configurations, a H^+_{surf} species is transferred to the C atom to form H_2COO^- (see Figure 3xxiii; note one of the H atoms that is bound to carbon is hidden to the eye). In our simulation, this H_2COO^{2-} species is subject to subsequent transformation into H_2COOH^-, which has received a second H^+_{surf} from ZnO. The H_2COOH^- species stay adsorbed on the Cu cluster in a similar bidentate mode (see Figure 3xxiii) or change into a monodentate one (see Figure 3xxiv). Such monodentate configurations at the Cu/ZnO interface represent the reactant state for the fifth pathway to give H_2CO in a near surface state, while at the same time leaving behind a H^+_{surf} species as well as a H adatom on Cu_8. The last pathway is a concerted one: It converts a $HCOO^-$ species adsorbed on the Cu cluster directly into H_2CO by dissociation of one C−O bond and a simultaneous hydrogen transfer reaction of a H adatom. The newly formed H_2CO desorbs into the near surface region, whereas the detached O atom remains adsorbed on the Cu cluster (see Figure 3xi).

In addition to these forward pathways, several back-reactions of H_2CO species were sampled. This included the formation of H_2COO^{2-} species, by the reaction of near surface H_2CO and an O adatom on Cu_8, as well as via adsorption of this near surface H_2CO species on a surface O atom of $ZnO(000\bar{1})$ which is located in close vicinity to the Cu cluster.

3.3. H_3CO^- and H_3COH Species. The formation of H_3CO^- species was sampled from a H_2CO species which, stemming from the near surface region (see Figure 3xi), physisorbs onto the Cu_8 cluster and abstracts an adjacent H adatom. The thus formed H_3CO^- species remains adsorbed in a bidentate mode on the Cu cluster via its oxygen atom (see Figure 3xiii).

Moreover, for the final product H_3COH there were two reaction pathways sampled, namely a direct one from the central H_2CO species and a second pathway via an H_3CO^- species. The direct pathway proceeds at the Cu/ZnO interface via an Eley−Rideal type of surface chemical reaction, which is visualized via a sequence of snapshots in Figure 5 and analyzed

DOI: 10.1021/acscatal.5b00442
ACS Catal. 2015, 5, 4201−4218

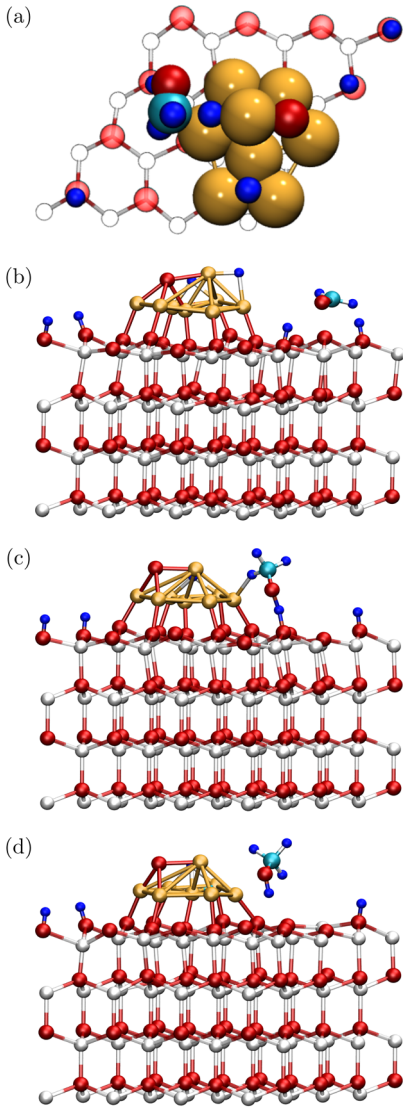

Figure 5. Methanol formation pathway from H_2CO via the Eley–Rideal type surface chemical reaction from a and b via c to d. Representative snapshots of C_1 species over the $Cu_8/ZnO(000\bar{1})$ nanocatalyst model are taken from the *ab initio* molecular dynamics trajectory underlying the metadynamics sampling of this part of the free energy landscape (see Figure 2a). (a) Top view of H_2CO in the reactant state according to Figure 3x. (b–d) Cu_8/ZnO catalyst slab model side view of the proceeding reaction, $H_2CO + 2H \rightarrow H_3COH$. Both in the reactant and in the product state, the C_1 species is neither covalently bound to the metal cluster nor to the oxide support, and therefore it is located in the near surface region over the catalyst surface (see subfigure b and d, respectively); see Table 2 for structural analysis. Only the crucial reaction step, see subfigure c, does involve covalent bonding of the reactant molecule to *both* the metal cluster and oxide support in order to abstract one H adatom and H^+_{surf} species from Cu_8 and ZnO, respectively. The same graphical representation as introduced in Figure 1 is used.

in terms of interatomic distances in Table 2. The corresponding reactant state is a H_2CO molecule in the near surface region over that nanocatalyst which only weakly interacts with H adatoms and H^+_{surf} species of Cu_8 and the ZnO surface, respectively, as depicted in snapshot Figure 3x and reproduced in Figure 5a and b. Both H species are transferred in a concerted mechanism to form H_3COH, see Figure 5c, which does not adsorb on the catalyst surface but stays in the near surface region (see Figure 3xvi and Figure 5d). Interestingly, only very recently we have obtained a similar Eley–Rideal mechanism for the final reaction step from H_2CO to H_3COH via "pathway" sampling of methanol synthesis from CO and over the reduced partially hydroxylated $ZnO(000\bar{1})$ surface.[117] In addition, for the same system another alternative pathway via H_3CO^- species, which is thermodynamically less preferred, was characterized to be a Langmuir–Hinshelwood type surface chemical reaction.[117] Likewise, in our present metadynamics exploration, the second reaction pathway leading to H_3CO^- was found to be such a Langmuir–Hinshelwood mechanism as well. This pathway starts with the C_1 species H_3CO^-, being adsorbed on Cu_8 (see Figure 3xiv), and a H_2O molecule stemming from the near surface region. In a physisorbed state, a H of this H_2O molecule is transferred to the C_1 species to give H_3COH and a OH adspecies (see Figure 3xviii). Once formed, the H_3COH molecule remains either physisorbed or adsorbed on Cu_8 (see Figure 3xvi and xvii, respectively). With an O adatom as a reaction partner, the H_3COH species decomposes back into H_3CO^-. Figure 3xv shows a snapshot of the product state of this reaction channel in which the hydrogen atom of the OH group was transferred to the adatom, whereas the H_3CO^- species remains adsorbed on the Cu cluster via its oxygen atom.

3.4. Side Reactions. In addition to those pathways that are directly related to methanol synthesis, our metadynamics simulations also explored competing reaction channels yielding side products and side species. On the one hand, these were methane formation as well as coking, which both were sampled over Cu_8. On the other hand, CO_3^{2-}, HCO_3^-, and H_2CO_3 (i.e., carbonate, bicarbonate, and carbonic acid, respectively) formation took place over the $ZnO(000\bar{1})$ surface part as well as at the Cu/ZnO interface of our catalyst model.

Carbonate species are formed from CO_2 stemming from the near surface region and the adsorption on a bare O atom of the ZnO surface (see Figure 3xxv; note in this snapshot the surface O atom is hidden from the eye by the C atom sitting directly above it). In a Mars–van Krevelen type of surface chemical reaction, these carbonate species create oxygen vacancies and start to migrate over the $ZnO(000\bar{1})$ surface while staying in a physisorbed state. Here, carbonate species further react with H^+_{surf} species to yield HCO_3^- that reside in physisorbed states over ZnO (see Figure 3xxvi). In a second pathway, a HCO_3^- species was formed from a physisorbed CO_3^{2-} on ZnO and a H atom of H_2O being adjacently adsorbed on a C atom of the Cu/ZnO interface. Two decomposition channels were sampled for such HCO_3^- species. In the first channel, it reacts with one H^+_{surf} species to give CO_2 and H_2O while leaving an O vacancy behind. Alternatively, when bound to a Cu atom at the Cu/ZnO interface, HCO_3^- species got further hydrogenated to H_2CO_3 which, residing in a physisorbed state over the ZnO surface, eventually decomposes into CO_2 and H_2O. However, our simulations did not generate pathways that turn carbonate species into formate and O adatoms over Cu as has been proposed earlier.[66,67]

Moreover, CH_x species with x ranging from zero to three (see Figure 3xxvii–xxx) were found to be synthesized via various reaction channels over Cu_8. The reaction network of Figure 4 summarizes these pathways with the species H_2COH^-, HCO^-, H_2CO, and H_3CO^- acting as reactants which all undergo C–O bond dissociation reactions. The corresponding degrees of freedom were accelerated by the CV c[C–O], whereas subsequent dehydrogenation reactions eventually leading toward isolated C atoms are driven by CV c[C–H].

DOI: 10.1021/acscatal.5b00442
ACS Catal. 2015, 5, 4201–4218

Table 2. Structural Characterization of the AIMD Snapshots Used to Depict Methanol Formation over the Cu_8/ZnO Catalyst via the Eley-Rideal Type Surface Chemical Reaction As Shown in Figure 5[a]

interatomic distances	H_2CO (Figure 5b)	H_2CO* (Figure 5c)	H_3COH (Figure 5d)
d_{Cu-H}	1.5	1.8	2.7
d_{C-H}	5.0	1.2	1.2
d_{O-H}	1.0	1.2	2.1
d_{O-H}	2.1	1.1	1.0
d_{C-Zn_s}	3.2	4.1	4.3

[a]The subscript "s" to the atomic symbols denotes atoms belonging to the topmost ZnO layer with the Zn_s atom being directly below the C_1 atom.

The corresponding back-reactions, i.e., formation of C−O and C−H bonds, were not further explored. The heterogeneous catalytic conversion of CO_2 and H_2 to CH_4 is achieved on an industrial scale via the well-known Fischer−Tropsch process, which is typically run over Ni catalysts which provide optimal yields.[156] Over Cu or the Cu/ZnO catalyst materials, methanation is a prominent side reaction in methanol synthesis from syngas. However, therein the high CO concentrations largely suppress this reaction.[61] CH_4 formation was not explored within our 3D metadynamics setup, though this side product species was generated in a preliminary 2D metadynamics simulation employing only two CVs, *i.e.*, c[C−H] and c[O−H]. In this simulation, except for replacing the CO_2 by a H_2CO molecule in the reactant state, we used essentially the same Cu_8/ZnO(000$\bar{1}$) catalyst model as shown in Figure 1. The analysis of the underlying 2D metadynamics simulation showed the formation of CH_4 from CH_2O adsorbed on Cu_8 and a H_2 molecule in the near surface region via an Eley−Rideal type surface chemical reaction. In the product state, CH_4 is found to desorb into the near surface region while an O adatom remains on the Cu cluster.

In summary, these results demonstrate the excellent capabilities of our computational scheme[116] based on molecular dynamics in generating a complete reaction network including also side reactions which are known to be present in the industrial process.

3.5. Active Role of Cu_8/ZnO(000$\bar{1}$). The present AIMD based simulation reveals mechanistically how the Cu_8/ZnO catalyst contributes to the overall reaction network of methanol synthesis from CO_2. Besides finite temperature effects, it is the direct interaction with C_1 species and side species in varying compositions which induces a manifold of different shapes, surface structure compositions, and, thus, changing redox properties of both the deposited highly dynamic Cu_8 cluster and the reduced ZnO support. In particular, our dynamical approach unfolded a very complex reaction space with additional putative active sites, SMSI effects, and eventually deactivation of catalyst material by oxidation. In the following, we discuss these effects on Cu_8/ZnO(000$\bar{1}$) with respect to the three main contributions: temperature, chemical interaction with C_1 species and adspecies, as well as the change in oxidation state of the catalyst material itself.

In the metadynamics simulations, the Cu_8 cluster is found to be a highly dynamic entity with continuous rearrangements of the individual Cu atoms and Cu migration events involving the quite fluxional Cu cluster. These fundamental phenomena originate from the shape of the deposited metal cluster, as we recently demonstrated by single point calculations and preliminary finite temperature AIMD simulations of representative Cu_8/ZnO(000$\bar{1}$) catalyst models.[25] Upon studying catalyzed oxidation of CO, a similar fluxional behavior was already found by AIMD for nanoscale gold catalysts when deposited on MgO.[157] More importantly, such dynamical behavior is not restricted to small clusters such as our Cu_8 model but was shown to be present also for Cu_n clusters with n > 600 on ZnO by preliminary MD simulations employing very accurate neural network potentials (as "learned from" DFT energies and forces).[158] However, we believe that the fluxional behavior of our catalyst model and the mesoscopic morphology changes of supported Cu particles as unveiled in seminal experiments[17,20] upon changing the environmental conditions, i.e. reducing versus oxidizing, are of different origin because of the vastly different size regimes even considering these larger computational Cu/ZnO models. In addition, we note that, for larger metal particles, properties such as persisting oxidation of extended facets or metallicity will be different compared to our Cu_8/ZnO model. Nonetheless, we expect our model to be well suitable for the present purpose in light of the fact that previous investigations have shown that catalytic activity sets in already for small clusters with nonmetallic properties[159] and, moreover, that small clusters are more reactive and can dominate the entire catalytic process even in the presence of lager particles.[129,160] Coming now back to our metadynamics simulations, the shape of the Cu cluster was observed to vary between 2D planar structures lying flat on the ZnO surface and more "spherical" 3D morphologies. The summary in Table 1 shows that in a flat morphology the Cu_8 cluster can have seven or eight Cu atoms in contact with ZnO (see, *e.g.*, Figure 3iii and xvii), while this number of these contacts is reduced to five for the more compact clusters (*e.g.*, see Figure 3iv). Migration of Cu atoms from the top of the Cu cluster to the Cu/ZnO interface and vice versa takes place to stabilize a certain product state (see, *e.g.*, Figure 3xxiii and xxiv as well as xxv and xxvi). Thus, the fluxionality of the catalytically active nanocluster and the stabilization of reaction intermediates and products is demonstrated to be intimately coupled!

Second, our simulation shows that in the presence of a strong interaction between C_1 species and Cu atoms, a spatial (re)distribution of some of these Cu atoms over the support material can take place. In particular, this is the case for CO species which easily form CO−Cu complexes. Once such a CO−Cu complex has been formed, the complete pathway of CO-assisted segregation, the diffusion of these complexes over the ZnO support (see Figure 3iv), as well as the recoalescence of these Cu atoms into the metal particles was sampled by our metadynamics simulations. Similar to these diffusion processes of CO−Cu complexes, our simulation sampled the separation of OH−Cu species from the Cu_8 cluster (see Figure 3xxvii) but not the migration of this complex over the ZnO surface. Note that the degrees of freedom that are responsible for these processes were not accelerated by the metadynamics algorithm but occurred in the sense of rare events on the time scale that is accessed by the underlying AIMD dynamics. Therefore, we can only provide order of magnitude estimates for the free energy

DOI: 10.1021/acscatal.5b00442
ACS Catal. 2015, 5, 4201−4218

Table 3. Structure and Redox State of C_1 Species over $Cu_8/ZnO(000\bar{1})$[a]

C_1 species	site	figure[b]	$d_{C-O,1(2)}$ (Å)	Δq_{C_1}	Δq_{Cu_8}	Δq_{ZnO}
CO_2	@Cu	Figure S3a	1.26 (1.27)	0.31	−0.09	−0.26
$HCOO^-$	@Cu	Figure S4a	1.22 (1.25)	0.16	0.05	−0.20
$HCOO^-$	@Cu(p)	Figure S5a	1.34 (1.34)	0.68	−0.08	−0.35
H_2COO^{2-}	@Cu(p)	Figure S6a	1.34 (1.37)	0.82	−0.39	−0.34
H_2COOH^-	@Cu	Figure S7a	1.45 (1.48)	1.37	−0.72	−0.55
H_2COOH^-	@ZnO	Figure S8a	1.51 (1.54)	0.89	−0.25	−0.89
H_2CO	near surface	Figure S9a	1.20	0.97	−0.40	−0.49
H_3COH	near surface	Figure S10a	1.42	1.43	−0.56	−0.68
H_3COH	@Cu	Figure S11a	1.60	1.28	−0.56	−0.48

[a]Representative snapshots were extracted from the AIMD trajectory underlying the metadynamics sampling. The positions of the C_1 species on the catalyst as well as desorbed states are indicated by @Cu, @ZnO, and near surface, whereas @Cu(p) denotes adsorption close to a perimeter site. Structural changes along the reduction process are monitored by the characteristic distance $d_{C-O,1(2)}$. The charge transfer parameter Δq (see text) was calculated for the C_1species, C atom and the two O atoms of the C_1 species, the Cu_8 cluster with adspecies, and the ZnO slab including the adsorbed H atoms and, if present, O vacancies, *i.e.*, Δq_{C_1}, Δq_{Cu_8}, and Δq_{ZnO}, respectively. Positive/negative values of Δq denote accumulations/depletion of electronic charge (reduction/oxidation) with respect to the reference structures: an isolated linear CO_2 and CO_2-free 1/2−H−sym-$Cu_8/ZnO(000\bar{1})$ surface model of Figure 1. [b]See Supporting Information.

barriers that govern the diffusion processes of CO−Cu on the partially hydroxylated $ZnO(000\bar{1})$ surface from the thermal energy k_BT(500 K), which corresponds to ∼43 meV. This value is much lower compared to the activation barriers calculated by static DFT calculations for CO and OH adspecies assisted Cu atom migration over low-index ZnO surfaces.[110] Similarly, CO-induced adatom sintering was investigated experimentally by scanning tunneling microscopy of a Pd−Fe_3O_4 model catalyst.[161] This study showed Pd−carbonyl species to facilitate coalescence of Pd adatoms, whereas Pd−OH species block the formation of clusters out of isolated Pd atoms. Having the focus clearly on the exploration of the global reaction network for methanol synthesis, our optimized simulation setup is not tailored to comprehensively and quantitative study such processes in the metal/oxide catalyst material itself. Yet, it allows us to find important aspects of such processes using our Cu_8/ZnO catalyst model. Therefore, it could be used in future metadynamics simulations once using CVs specifically tailored[116,117] to study CO−Cu and OH−Cu migration. Such simulations would address and disclose the mechanisms of the formation of the catalytically active Cu/ZnO morphologies under reaction conditions as well as catalyst deactivation. In addition, migration of Cu atoms at the Cu/ZnO interface may also stabilize certain reactant and product states of C_1 species, *e.g.*, $H_2COO_2^-$ (see Figure 3xxiii and xxiv).

Third, the structure and electronic properties of the $Cu_8/ZnO(000\bar{1})$ model are subject to dynamic changes which occur in direct response to the interaction with C_1 species and adspecies as well as in some reaction channels due to the formation of (adsorbed) side species. To complete the reduction process of one CO_2 molecule toward methanol, the $Cu_8/ZnO(000\bar{1})$ catalyst must provide electronic charge to the C_1 species in addition to four H species and abstraction of one O atom. The progress of such electronic charge transfer is demonstrated by the increasing values of the Δq_{C_1} parameters, which were calculated for a representative set of AIMD snapshots underlying our metadynamics sampling (see Table 3). Consequently, at the same time, the redox state of our catalyst model changes from strongly reduced to fully oxidized as indicated by the decreasing values of the electronic charge difference Δq_{Cu_8} and Δq_{ZnO} (see Table 3 and section 3 in the Supporting Information. Acting in concert, these changes in surface composition and oxidation state alter the overall balance of the underlying surface stabilization mechanisms at work, i.e., hydroxylation of $ZnO(000\bar{1})$, O vacancy creation, Cu−Cu cohesion, Zn−Cu alloying, and ZnO migration onto Cu,[24,25] and, therefore, give rise to many different catalyst surface structures and morphologies. Table 1 and Figure 3 summarize the broad variations of the $Cu_8/ZnO(000\bar{1})$ structures which have been generated by the AIMD trajectory underlying our metadynamics sampling of the FES. Interestingly, these structural variations comprise a huge space of possibilities which goes far beyond the degrees of freedom associated with the chemical reactions of the C_1 species that were explicitly accelerated by the three CVs to enhance their sampling. A detailed discussion of all these effects on the electronic structure of C_1 species and the catalyst model is presented in section 3 in the Supporting Information for selected AIMD snapshots. In particular, this includes the wetting/dewetting behavior of the Cu_8 cluster as well as the adsorbate and adatom decoration of $Cu_8/ZnO(000\bar{1})0001$.

In the following, we have picked the most striking example, which is the spontaneous creation of O vacancies, because it demonstrates the presence of a dynamic SMSI effect in the $Cu_8/ZnO(000\bar{1})$ model that has been revealed by metadynamics sampling. In our metadynamics simulation, this is seen to take place once the reduction reaction has consumed larger amounts of H species from the $ZnO(000\bar{1})$ surface such that the overall H coverage on the catalyst had decreased below 1/4 ML. It is well established that both thermodynamically and electronically such a surface composition is highly unstable.[24,25] However, in the simulation the intrinsic stability of the surface with such low hydrogen coverage is recovered by the immediate creation of O vacancies (see, *e.g.*, Figure 3xiv, xv, and xviii). According to our calculated phase diagrams, this becomes the relevant mechanism to compensate for the structural and electronic instability of the polar $ZnO(000\bar{1})$ surface.[24,25] Note that for our particular catalyst model, $Cu_8/ZnO(000\bar{1})$, one O vacancy is equivalent to two H adspecies on the ZnO surface in the sense of this stabilization. Besides the mechanisms via H_2O formation, *vide supra*, in our metadynamics exploration O vacancies are created via self-migration of one O atom of the top $ZnO(000\bar{1})$ surface layer onto the Cu_8 cluster, thus giving rise to O adatoms (see, *e.g.*, Figure S11 in the Supporting Information) or to OH adspecies after

DOI: 10.1021/acscatal.5b00442
ACS Catal. 2015, 5, 4201−4218

subsequent reaction of these O atoms with H adspecies from Cu_8. Although the generation of O vacancies leads to (re)reduction of the ZnO(000$\bar{1}$) surface,[25] at the same time these O adatoms and OH adspecies on the Cu_8 cluster lead to its oxidation (see Table 3 and section 3 in the Supporting Information). Therefore, in the catalytic cycle such oxidized Cu clusters will be partially deactivated. In principle, there should exist reaction channels, *e.g.*, via the formation of H_2O, which would allow for the removal of these O adatoms and OH adspecies (see, *e.g.*, Figure 3xiii and viii, respectively). None of these nor similar channels were explored by our metadynamics simulation. This seems to be in correspondence with very recent XPS experiments showing a persisting oxidation of about 75% of the Cu surface atoms (+II oxidation state) after catalyst rereduction and, therefore, point to sustained morphological changes of the catalyst material which promote the stabilization of Cu in different oxidation states.[23] According to the insights generated by our present simulation, these morphological changes could be related to the creation of O vacancies or Cu dispersion mediated by CO.

Certainly, in contrast to the industrial process, our present AIMD setup does not allow for an on-the-fly insertion (or removal) of reactants in the sense of grand canonical equilibrium with suitable reservoirs for these molecules. Therefore, there might still exist reaction steps which require the interaction of gas phase and catalyst, *e.g.*, (re)reduction via continuous H_2 adsorption. Addressing this issue of the coupling of environment and catalyst surface introduced a stepwise approach which we have implemented only very recently in our computational study of methanol synthesis on bare ZnO as the final step.[116,117] This step is designed to compute the thermochemistry and kinetics of the individual reaction steps of the most probable reaction pathways in the reaction network.[116,117] As for the current study, i.e., the exploration of the global network for methanol production (and its back-reactions) on the much more complex Cu/ZnO catalyst, we were only interested in localizing all open pathways and species; it was largely sufficient to use a single model which could facilitate the full reduction process[115,116] from CO_2 to methanol, *vide supra*. In addition, having an oxidized Cu_8/ZnO(000$\bar{1}$) catalyst model in the product state is even more realistic for the subsequent metadynamics sampling of the back-reaction, i.e., methanol decomposition.

3.6. H_2CO over Reduced Cu_8/ZnO(000$\bar{1}$): First Insights. It turned out that in our metadynamics simulations the sampling of back-reactions became very inefficient, as in many cases the involved degrees of freedom were not accelerated by one of the CVs. In addition, if larger barriers are involved, these reactions became also virtually irreversible given accessible on-the-fly simulation time scales. For example, both reactants and reaction active sites became spatially separated in the forward reaction, *e.g.*, O adatoms and C_1-species and H_2O and an O vacancy, respectively, and thus were "unavailable" for any back-reaction. This was particularly the case for the sampling of regions on the free energy landscape of Figure 2a with C_1 species being hydrogenated to a large degree, i.e., H_2COH, H_3CO^-, and H_3COH. In this stage of the simulation, the Cu_8/ZnO(000$\bar{1}$) surface structure had substantially changed due to the accompanying oxidation of the catalyst, *vide supra*.

To overcome these sampling limitations in the original setup, we have prepared and started a second 3D metadynamics run using the same setup and Cu_8/ZnO(000$\bar{1}$) catalyst model as for our exploration (see Figure 1), but having exchanged CO_2 by a H_2CO molecule in the reactant state (see Figure 6a). Compared to the old setup, this change of the reactant species

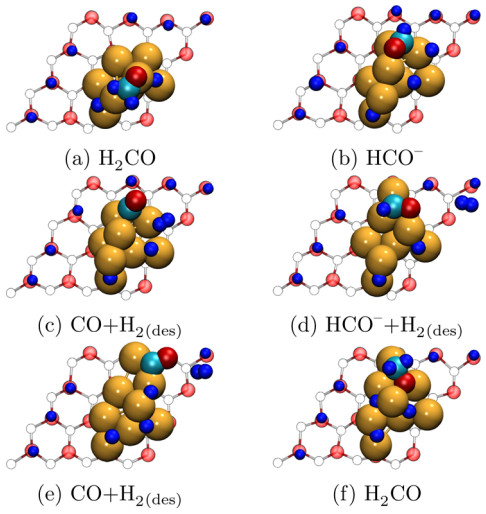

Figure 6. Representative snapshots of the explorative three-dimensional metadynamics simulation using a rereduced Cu/ZnO(000$\bar{1}$)-0001 catalyst model and a H_2CO reactant (see subfigure a). The subfigure captions (a–f) identify the C_1 species by their chemical formula. The same color code as defined in Figure 3 is used. The label "des" in the subcaptions denotes transiently desorbed species in the near surface region over the catalyst. Chemical formulas are assigned according to formal charges of closed shell gas phase species.

in the system increased the total number of H atoms by two and reduced the number of O atoms by one, which, effectively, is nothing but a rereduction of the catalyst model (see ref 116). This second metadynamics simulation has generated only preliminary insights, but so far, we could extract putative new reactions pathways which, *inter alia*, actively involve species in the near surface region over the Cu_8/ZnO(000$\bar{1}$) catalyst. Starting from the initial structure, our analysis of the AIMD trajectory shows that the adsorbed H_2CO species decomposes on Cu_8 into HCO^- (see Figure 6a and b). In a second step, this species reacts further with a H adatom forming CO and a H_2 molecule (see Figure 6c). While the H_2 is subsequently desorbing into the near surface region over the surface, the CO species is found to reside on the Cu cluster.

Furthermore, CO species can act as mediators for the transfer of H species from the ZnO surface onto the Cu_8 cluster via a HCO^- intermediate species (see Figure 6c, d, and e). This demonstrates an additional active role of CO in the C_1 reduction process over Cu_8. Furthermore, our sampling unveiled a new reaction channel for the reduction of CO by a H_2 molecule of the near surface region to directly give H_2CO via an Eley–Rideal type of surface chemical reaction (see Figure 6.e and Sec. 6.f). Only very recently, we have disclosed such type of reactions to be key to the overall reaction mechanism of methanol synthesis when performed over a Cu-free and strongly reduced ZnO catalyst surface.[117]

3.7. Comparison to Mechanisms Proposed for Bare Cu. Our AIMD based approach has established a global reaction network which features a very rich pattern of both species and chemical transformations underlying the process of methanol synthesis over a realistic Cu_8/ZnO(000$\bar{1}$) catalyst model. Yet, up until most recently[57,58] other theoretical works have used low-index Cu surfaces, Cu/Zn surface alloys, and

DOI: 10.1021/acscatal.5b00442
ACS Catal. 2015, 5, 4201–4218

unsupported Cu clusters as simplified catalyst models to study the mechanism of methanol synthesis from CO_2. These computational studies employed the usual static and step-by-step procedure of localizing minima structures of some putative active species on the PES by geometry optimization techniques, mapping of minimum energy pathways interconnecting these minima typically using NEB-type approaches, carefully narrowing down transition states, and finally estimating thermodynamic corrections by virtue of harmonic analysis using the optimized structures.[6,81−85,88] Applying this traditional approach to low-index Cu surfaces and unsupported Cu clusters, three different reaction mechanisms were proposed: the so-called $HCOO^-$, CO, and $COOH^+$ based mechanisms (for a recent review see ref 77). In Table 4, we have summarized these mechanisms and show all species that are involved along the proposed reaction pathways that are labeled I, II, and III, respectively. In addition, Table 4 lists all species which were "synthesized" by our present AIMD-based approach upon exploring the global reaction network over the $Cu_8/ZnO(000\bar{1})$ nanocatalyst. For the sake of comparison, our previous AIMD-based results for methanol synthesis over Cu-free, defective $ZnO(000\bar{1})$ catalyst models[115,116] are also included in the table (denoted as "ZnO"). As one can immediately recognize, methanol synthesis on both catalyst materials, Cu/ZnO and ZnO, involve the same set of species; however, the sampled reaction channels that interconnect these are significantly different on the two catalysts.

Table 4. Comparison of C_1 Species That Have Been Suggested in the Literature for Three Potential Mechanisms (Labeled I, II, and III) of Methanol Synthesis over Low-Index Cu Surfaces and Unsupported Cu Clusters Based on State of the Art (Static) Computational Approaches Compared to the Species That Have Been "Synthesized" by Our Computational Approach Employing Advanced *ab Initio* Molecular Dynamics Techniques (AIMD) and More Realistic Catalyst Models Cu/ZnO and ZnO Surfaces[a]

	static DFT			reaction networks from AIMD	
Species	I	II	III	Cu_8/ZnO (this work)	ZnO (from Ref. 115–117)
CO_2	✗	✗	✗	✗	✗
$COOH^+$		✗	✗	✗	✗
COHOH			✗		
CO		✗		✗	✗
COH^+			✗	✗	✗
$HCOO^-$	✗			✗	✗
HCOOH				✗	✗
HCO^-		✗		✗	✗
HCOH		✗	✗	✗	✗
H_2COO^{2-}	✗			✗	✗
H_2COOH^-	✗			✗	✗
H_2CO	✗			✗	✗
H_2COH^-		✗	✗	✗	✗
H_3CO^-	✗			✗	✗
H_3COH	✗	✗	✗	✗	✗

[a]The three main reaction mechanisms over Cu are the $HCOO^-$ mechanism, the CO hydrogenation mechanism, and the $COOH^+$ mechanism being labeled I, II, and III, respectively (see ref 77). Species of the reaction networks of methanol synthesis over $ZnO(000\bar{1})$ supported Cu_8 nanocatalysts (this work) and over defective pure $ZnO(000\bar{1})$ surfaces (see refs 115, 116, 117).

According to the $HCOO^-$ mechanism (I), methanol is formed from CO_2 by a successive chain of hydrogenation reactions and one C−O bond scission via $HCOO^-$, H_2COO^{2-}, H_2COOH^-, and H_2CO species, respectively. This reaction channel is part of our reaction network, which, in addition, also predicts a direct pathway from $HCOO^-$ to H_2CO on the Cu cluster itself. More importantly, over our $Cu_8/ZnO(000\bar{1})$ catalyst model, the final reaction step proceeds via an Eley−Rideal type of surface reaction. Herein, a H_2CO species in the near surface region over our catalyst model gets hydrogenated at the Cu/ZnO interface by abstracting one H atom from each part of the surface, whereas the final product methanol also remains in the near surface region. A direct conversion of H_2COO^{2-} into H_3COO^- over bare, ZnO-free Cu catalysts was suggested based on kinetic arguments[162] and proposed to take place via a concerted mechanism,[83] thus avoiding formation of a relatively weakly bound formaldehyde species on bare copper catalysts. This mechanism is absent from our reaction network that has been generated on Cu/ZnO. Furthermore, over the Cu-type catalysts, the CO mechanism (II) is proposed to proceed via the chemical species CO_2, $COOH^+$, CO, HCO^-, HCOH, and H_2COH^-. These species were all sampled in our metadynamics exploration of reaction network. Only the final interconversion of H_2COH^- directly into methanol is missing from our reaction network. We suspect this species to be a spectator species on the Cu/ZnO catalyst similar to the situation disclosed in the refined reaction network of methanol synthesis over the Cu-free, bare ZnO catalyst.[117] Finally, the species relevant to the $COOH^+$ mechanism (III) are very similar to those involved in the CO mechanism. In addition to the common species $COOH^+$, HCOH, and H_2COH^-, the $COOH^+$ mechanism includes also COH^+ and the COHOH intermediate. The latter species (COHOH), however, was the only one proposed in the literature which is absent in our sampling although all the necessary degrees of freedom driving this reaction were explicitly included in the tree CVs.

Nonetheless, despite the astonishingly good agreement in terms of species, there exist significant differences in the individual reaction steps between the ones proposed according to the three mechanisms over low-index Cu surfaces and isolated Cu clusters and those which have been "synthesized" via our AIMD molecular dynamics approach in conjunction with a quite realistic model of a supported, about one nanometer large, metal cluster for the Cu/ZnO catalyst. In particular, these differences arise from the presence of multiple, most substantial effects, which, apart from finite temperature and thus thermal activation, are only present when the combined Cu/ZnO nanocatalyst system consisting of a metal cluster on an oxide support is used for the calculations. These effects, which we all consider in the present study, include (i) the active role of the defective ZnO surface as well as the Cu/ZnO interface depending on the thermodynamic state of the gas phase, (ii) the highly dynamical character of the Cu cluster, which gives rise to various active morphologies that can stabilize reactant, intermediate, and product states of the involved C_1 species in intricate ways, (iii) charge transfer effects over the metal/support interface in particular for the activation of the reactant CO_2,[24,25] and (iv) the consistent inclusion of chemical reactions that involve or fully take place in the near surface region at the interface of catalyst and gas phase, and last but certainly not least (v) the presence of SMSI effects along all pathways. We believe that this level of modeling can only be reached when using the "molecular dynamics approach to theoretical heterogeneous catalysis."[115,116]

DOI: 10.1021/acscatal.5b00442
ACS Catal. 2015, 5, 4201−4218

4. SUMMARY

In this work, we have employed advanced *ab initio* molecular dynamics sampling techniques in order to shed light on the intricate interplay of both the complex scenario of surface chemical reactions and dynamically changing catalyst morphologies using thermodynamically optimized Cu/ZnO nanocatalyst models. This attempts to take into account systematically what happens at the elevated temperature and pressure conditions as required by the industrial heterogeneous catalytic process of methanol synthesis from syngas. Optimized with respect to the relevant thermodynamic conditions of the gas phase, a Cu_8/ZnO catalyst surface model has been designed to explore the gross free energy landscape of chemical transformations of molecular C_1 species from CO_2 toward methanol. Our "molecular dynamics approach to theoretical heterogeneous catalysis"[115,116] is found to generate, automatically by itself, a rich network of parallel, competing, and reverse reaction pathways over a *lively* Cu/ZnO catalyst surface. It is found to generate active sites and explores their role in the context of catalyzed chemical transformations of C_1 species over all parts of the catalyst model, including dynamic SMSI effects as well as electronic charge transfer over the Cu/ZnO interface, all being crucial for molecular activation. Moreover, having "synthesized" more than 20 previously discussed C_1 species in addition to side species and adspecies decorations on Cu, highly reactive formaldehyde could be identified to be the key intermediate toward methanol formation on Cu/ZnO. Moreover, several well-known side reactions, such as reverse and forward water−gas shift reactions, coking, and methanation, are all included in the global reaction network as generated by molecular dynamics. Within the full network, three archetypal mechanisms of surface chemical reactions, namely, (i) Eley−Rideal, (ii) Langmuir−Hinshelwood, and (iii) Mars−van Krevelen types, were generated by *ab initio* metadynamics sampling of the free energy landscape and were subsequently identified from analyzing the individual reaction steps based on the underlying *ab initio* molecular dynamics trajectories. It is stressed that the former mechanism can only be captured upon taking into account systematically the near surface region at the interface of catalyst and gas phase as an active reaction space. The latter mechanism, on the other hand, can only be realized in a calculation once catalyst sites, be it atoms or vacancies, are systematically included in chemical reactions that involve all reacting molecular species. In particular, processes like oxygen vacancy creation via water formation and hydrogen spillover from ZnO onto Cu mediated by dynamically migrating CO molecules demonstrate the active role of molecular species in promoting the catalyst toward activated states. Last but not least, our simulations also provided molecular insight into mechanisms that lead to catalyst deactivation such as coking.

After having obtained a rich catalog of putative reaction pathways, species, and active catalyst morphologies, we could continue in future work with the final step of our computational scheme to heterogeneous catalysis. By employing pathway-tailored sets of collective variables, the free energy profile of all individual pathways will eventually provide all thermodynamic and kinetic data to construct the global reaction network of methanol synthesis over Cu_8/ZnO. For the Cu-free, bare ZnO catalyst, we have previously demonstrated our automated "molecular dynamics approach to theoretical heterogeneous catalysis"[115,116] to be a powerful, robust, and flexible computational tool to get a handle on chemical reactions and processes in complex setups, which applies not only to gas−solid[115,116] but in particular to liquid−solid[139,163−167] interfaces.

■ ASSOCIATED CONTENT

Supporting Information

The Supporting Information is available free of charge on the ACS Publications website at DOI: 10.1021/acscatal.5b00442.

Additional characterization of the free energy landscape and molecular species from the AIMD trajectories via automated procedures using structural motifs and the analysis of the electronic structure and redox state of AIMD snapshots (PDF)

■ AUTHOR INFORMATION

Corresponding Author

*Phone: +49 (0)234 322 6750. Fax: +49 (0)231 4045. E-mail: johannes.frenzel@theochem.rub.de.

Notes

The authors declare no competing financial interest.

■ ACKNOWLEDGMENTS

This work has been supported by the German Research Foundation (DFG) via the Cluster of Excellence EXC 1069 "RESOLV" and by the Research Department "Interfacial Systems Chemistry" (IFSC) funded by RUB. Computational resources were provided by SuperMUC (München) as well as by HPC−RESOLV and BOVILAB@RUB (Bochum).

■ REFERENCES

(1) Thomas, J. M.; Thomas, W. J. *Principles and Practice of Heterogeneous Catalysis*; Wiley-VCH: Weinheim, Germany, 1996.
(2) Olah, G. A. *Angew. Chem., Int. Ed.* **2005**, *44*, 2636−2639.
(3) Welcome − Methanol Institute. www.methanol.org (accessed Nov. 3, 2014).
(4) Davies, P.; Snowdon, F. F.; Bridger, G.; Hughes, D. O.; Young, P. W. U.K. Patent 1010871, 1965.
(5) Kasatkin, I.; Kurr, P.; Kniep, B.; Trunschke, A.; Schlögl, R. *Angew. Chem.* **2007**, *119*, 7465−7468.
(6) Behrens, M.; Studt, F.; Kasatkin, I.; Kühl, S.; Hävecker, M.; Abild-Pedersen, F.; Zander, S.; Girgsdies, F.; Kurr, P.; Kniep, B.-L.; Tovar, M.; Fischer, R. W.; Nørskov, J. K.; Schlögl, R. *Science* **2012**, *336*, 893−897.
(7) Behrens, M.; Zander, S.; Kurr, P.; Jacobsen, N.; Senker, J.; Koch, G.; Ressler, T.; Fischer, R. W.; Schlögl, R. *J. Am. Chem. Soc.* **2013**, *135*, 6061−6068.
(8) Kagan, Y. B.; Liberov, L. G.; Slivinskii, E. V.; Loktev, S. M.; Lin, G. I.; Rozovskii, A. Y.; Bashkirov, A. N. *Dokl. Akad. Nauk SSSR, Ser. Khim.* **1975**, *221*, 1093−1095.
(9) Kagan, Y. B.; Rozovskii, A. Y.; Liberov, L. G.; Slivinskii, E. V.; Lin, G. I.; Loktev, S. M.; Bashkirov, A. N. *Dokl. Akad. Nauk SSSR, Ser. Khim. (Eng.)* **1975**, *224*, 1081−1084.
(10) Chinchen, G.; Denny, P.; Parker, D.; Spencer, M.; Whan, D. *Appl. Catal.* **1987**, *30*, 333−338.
(11) Liu, G.; Willcox, D.; Garland, M.; Kung, H. H. *J. Catal.* **1985**, *96*, 251−260.
(12) Muhler, M.; Toernqvist, E.; Nielsen, L. P.; Clausen, B. S.; Topsøe, H. *Catal. Lett.* **1994**, *25*, 1−10.
(13) Schack, C. J.; McNeil, M. A.; Rinker, R. G. *Appl. Catal.* **1989**, *50*, 247−263.
(14) Kung, H. H. *Catal. Rev.: Sci. Eng.* **1980**, *22*, 235−259.
(15) Chorkendorff, I.; Niemantsverdriet, J. W. *Concepts of Modern Catalysis and Kinetics*; Wiley-VCH: Weinheim, Germany, 2007.
(16) Waugh, K. *Catal. Lett.* **2012**, *142*, 1153−1166.
(17) Clausen, B. S.; Schiøtz, J.; GrÅbæk, L.; Ovesen, C. V.; Jacobsen, K. W.; Nørskov, J. K.; Topsøe, H. *Top. Catal.* **1994**, *1*, 367−376.

DOI: 10.1021/acscatal.5b00442
ACS Catal. 2015, 5, 4201−4218

(18) Grunwaldt, J. D.; Molenbroek, A. M.; Topsøe, N. Y.; Topsøe, H.; Clausen, B. S. *J. Catal.* **2000**, *194*, 452−460.
(19) Günter, M.; Ressler, T.; Bems, B.; Büscher, C.; Genger, T.; Hinrichsen, O.; Muhler, M.; Schlögl, R. *Catal. Lett.* **2001**, *71*, 37−44.
(20) Hansen, P. L.; Wagner, J. B.; Helveg, S.; Rostrup-Nielsen, J. R.; Clausen, B. S.; Topsøe, H. *Science* **2002**, *295*, 2053−2055.
(21) Liu, J. J. *ChemCatChem* **2011**, *3*, 934−948.
(22) Kandemir, T.; Girgsdies, F.; Hansen, T. C.; Liss, K.-D.; Kasatkin, I.; Kunkes, E. L.; Wowsnick, G.; Jacobsen, N.; Schlögl, R.; Behrens, M. *Angew. Chem., Int. Ed.* **2013**, *52*, 5166−5170.
(23) Martin, O.; Perez-Ramirez, J. *Catal. Sci. Technol.* **2013**, *3*, 3343−3352.
(24) Martínez-Suárez, L.; Frenzel, J.; Marx, D.; Meyer, B. *Phys. Rev. Lett.* **2013**, *110*, 086108.
(25) Martínez-Suárez, L.; Frenzel, J.; Marx, D. *Phys. Chem. Chem. Phys.* **2014**, *16*, 26119−26136.
(26) Tauster, S. J.; Fung, S. C.; Garten, R. L. *J. Am. Chem. Soc.* **1978**, *100*, 170−175.
(27) Foger, K. *Catalysis: Science and Technology*; Springer-Verlag: Berlin, 1984.
(28) Kurtz, M.; Bauer, N.; Buescher, C.; Wilmer, H.; Hinrichsen, O.; Becker, R.; Rabe, S.; Merz, K.; Driess, M.; Fischer, R. A.; Muhler, M. *Catal. Lett.* **2004**, *92*, 49−52.
(29) Hadden, R.; Sakakini, B.; Tabatabaei, J.; Waugh, K. *Catal. Lett.* **1997**, *44*, 145−151.
(30) Topsøe, N.-Y.; Topsøe, H. *Top. Catal.* **1999**, *8*, 267−270.
(31) Wilmer, H.; Hinrichsen, O. *Catal. Lett.* **2002**, *82*, 117−122.
(32) Kanai, Y.; Watanabe, T.; Fujitani, T.; Uchijima, T.; Nakamura, J. *Catal. Lett.* **1996**, *38*, 157−163.
(33) Spencer, M. *Catal. Lett.* **1999**, *60*, 45−49.
(34) Liao, F.; Huang, Y.; Ge, J.; Zheng, W.; Tedsree, K.; Collier, P.; Hong, X.; Tsang, S. C. *Angew. Chem., Int. Ed.* **2011**, *50*, 2162−2165.
(35) Fichtl, M. B.; Schumann, J.; Kasatkin, I.; Jacobsen, N.; Behrens, M.; Schlögl, R.; Muhler, M.; Hinrichsen, O. *Angew. Chem., Int. Ed.* **2014**, *53*, 7043−7047.
(36) Nakamura, J.; Nakamura, I.; Uchijima, T.; Kanai, Y.; Watanabe, T.; Saito, M.; Fujitani, T. *J. Catal.* **1996**, *160*, 65−75.
(37) Nakamura, J.; Uchijima, T.; Kanai, Y.; Fujitani, T. *Catal. Today* **1996**, *28*, 223−230.
(38) d'Alnoncourt, R. N.; Kurtz, M.; Wilmer, H.; Löffler, E.; Hagen, V.; Shen, J.; Muhler, M. *J. Catal.* **2003**, *220*, 249−253.
(39) Naumann d' Alnoncourt, R.; Xia, X.; Strunk, J.; Löffler, E.; Hinrichsen, O.; Muhler, M. *Phys. Chem. Chem. Phys.* **2006**, *8*, 1525−1538.
(40) Schimpf, S.; Rittermeier, A.; Zhang, X.; Li, Z.-A.; Spasova, M.; van den Berg, M. W. E.; Farle, M.; Wang, Y.; Fischer, R. A.; Muhler, M. *ChemCatChem* **2010**, *2*, 214−222.
(41) Zander, S.; Kunkes, E. L.; Schuster, M. E.; Schumann, J.; Weinberg, G.; Teschner, D.; Jacobsen, N.; Schlögl, R. R.; Behrens, M. *Angew. Chem., Int. Ed.* **2013**, *52*, 6536−6540.
(42) Schott, V.; Oberhofer, H.; Birkner, A.; Xu, M.; Wang, Y.; Muhler, M.; Reuter, K.; Wöll, C. *Angew. Chem., Int. Ed.* **2013**, *52*, 11925−11929.
(43) Spencer, M. *Surf. Sci.* **1987**, *192*, 323−328.
(44) Spencer, M. *Surf. Sci.* **1987**, *192*, 329−335.
(45) Spencer, M. *Surf. Sci.* **1987**, *192*, 336−343.
(46) Fujitani, T.; Nakamura, J. *Catal. Lett.* **1998**, *56*, 119−124.
(47) Nakamura, J.; Choi, Y.; Fujitani, T. *Top. Catal.* **2003**, *22*, 227.
(48) Liu, Z.; Rittermeier, A.; Becker, M.; Kahler, K.; Löffler, E.; Muhler, M. *Langmuir* **2011**, *27*, 4728−4733.
(49) Liao, F.; Zeng, Z.; Eley, C.; Lu, Q.; Hong, X.; Tsang, S. C. *Angew. Chem., Int. Ed.* **2012**, *51*, 5832−5836.
(50) Burch, R.; Golunski, S. E.; Spencer, M. S. *J. Chem. Soc., Faraday Trans.* **1990**, *86*, 2683−2691.
(51) Spencer, M. *Catal. Lett.* **1998**, *50*, 37−40.
(52) Spencer, M. *Top. Catal.* **1999**, *8*, 259−266.
(53) Wagner, J. B.; Hansen, P. L.; Molenbroek, A. M.; Topsøe, H.; Clausen, B. S.; Helveg, S. *J. Phys. Chem. B* **2003**, *107*, 7753−7758.
(54) Natesakhawat, S.; Lekse, J. W.; Baltrus, J. P.; Ohodnicki, P. R.; Howard, B. H.; Deng, X.; Matranga, C. *ACS Catal.* **2012**, *2*, 1667−1676.
(55) van den Berg, M.; Polarz, S.; Tkachenko, O.; Kähler, K.; Muhler, M.; Grünert, W. *Catal. Lett.* **2009**, *128*, 49−56.
(56) García-Trenco, A.; Martínez, A. *Catal. Today* **2013**, *215*, 152−161.
(57) García-Muelas, R.; Li, Q.; López, N. *ACS Catal.* **2015**, *5*, 1027−1036.
(58) Back, S.; Kim, H.; Jung, Y. *ACS Catal.* **2015**, *5*, 965−971.
(59) Kurtz, M.; Bauer, N.; Wilmer, H.; Hinrichsen, O.; Muhler, M. *Chem. Eng. Technol.* **2004**, *27*, 1146−1150.
(60) Baltes, C.; Vukojević, S.; Schüth, F. *J. Catal.* **2008**, *258*, 334−344.
(61) Klier, K.; Chatikavanij, V.; Herman, R. G.; Simmons, G. W. *J. Catal.* **1982**, *74*, 343−360.
(62) Chinchen, G.; Denny, P.; Jennings, J.; Spencer, M.; Waugh, K. *Appl. Catal.* **1988**, *36*, 1−65.
(63) Kurtz, M.; Wilmer, H.; Genger, T.; Hinrichsen, O.; Muhler, M. *Catal. Lett.* **2003**, *86*, 77−80.
(64) Chinchen, G. C.; Spencer, M. S.; Waugh, K. C.; Whan, D. A. *J. Chem. Soc., Faraday Trans. 1* **1987**, *83*, 2193−2212.
(65) Bowker, M.; Hadden, R. A.; Houghton, H.; Hyland, J. N. K.; Waugh, K. C. *J. Catal.* **1988**, *109*, 263−273.
(66) Millar, G. J.; Rochester, C. H.; Waugh, K. C. *J. Chem. Soc., Faraday Trans.* **1992**, *88*, 1033−1039.
(67) Bailey, S.; Froment, G.; Snoeck, J.; Waugh, K. *Catal. Lett.* **1994**, *30*, 99−111.
(68) Sakakini, B.; Tabatabaei, J.; Watson, M. J.; Waugh, K. C.; Zemicael, F. W. *Faraday Discuss.* **1996**, *105*, 369−376.
(69) Wachs, I. E.; Madix, R. J. *J. Catal.* **1978**, *53*, 208−227.
(70) Ying, D. H.; Robert, J. *J. Catal.* **1980**, *61*, 48−56.
(71) Bowker, M.; Houghton, H.; Waugh, K. C. *J. Chem. Soc., Faraday Trans. 1* **1981**, *77*, 3023−3036.
(72) Ortelli, E.; Weigel, J.; Wokaun, A. *Catal. Lett.* **1998**, *54*, 41−48.
(73) Weigel, J.; Koeppel, R. A.; Baiker, A.; Wokaun, A. *Langmuir* **1996**, *12*, 5319−5329.
(74) Yang, Y.; Mims, C.; Disselkamp, R.; Mei, D.; Kwak, J.-H.; Szanyi, J.; Peden, C.; Campbell, C. *Catal. Lett.* **2008**, *125*, 201−208.
(75) Clarke, D.; Lee, D.; Sandoval, M.; Bell, A. *J. Catal.* **1994**, *150*, 81−93.
(76) Millar, G. J.; Rochester, C. H.; Howe, C.; Waugh, K. C. *Mol. Phys.* **1992**, *76*, 833−849.
(77) Appel, A. M.; Bercaw, J. E.; Bocarsly, A. B.; Dobbek, H.; DuBois, D. L.; Dupuis, M.; Ferry, J. G.; Fujita, E.; Hille, R.; Kenis, P. J. A.; Kerfeld, C. A.; Morris, R. H.; Peden, C. H. F.; Portis, A. R.; Ragsdale, S. W.; Rauchfuss, T. B.; Reek, J. N. H.; Seefeldt, L. C.; Thauer, R. K.; Waldrop, G. L. *Chem. Rev.* **2013**, *113*, 6621−6658.
(78) Hu, Z.-M.; Takahashi, K.; Nakatsuji, H. *Surf. Sci.* **1999**, *442*, 90−106.
(79) Catlow, C. R. A.; French, S. A.; Sokol, A. A.; Thomas, J. M. *Philos. Trans. R. Soc., A* **2005**, *363*, 913−936.
(80) Morikawa, Y.; Iwata, K.; Terakura, K. *Appl. Surf. Sci.* **2001**, *169-170*, 11−15.
(81) Yang, Y.; Evans, J.; Rodriguez, J. A.; White, M. G.; Liu, P. *Phys. Chem. Chem. Phys.* **2010**, *12*, 9909−9917.
(82) Grabow, L. C.; Mavrikakis, M. *ACS Catal.* **2011**, *1*, 365−384.
(83) Sakong, S.; Mosch, C.; Lozano, A.; Busnengo, H. F.; Groß, A. *ChemPhysChem* **2012**, *13*, 3467−3471.
(84) Yang, Y.; White, M. G.; Liu, P. *J. Phys. Chem. C* **2012**, *116*, 248−256.
(85) Studt, F.; Abild-Pedersen, F.; Varley, J.; Nørskov, J. K. *Catal. Lett.* **2013**, *143*, 71−73.
(86) Zhao, Y.-F.; Yang, Y.; Mims, C.; Peden, C. H.; Li, J.; Mei, D. *J. Catal.* **2011**, *281*, 199−211.
(87) Yang, Y.; Mims, C.; Mei, D.; Peden, C.; Campbell, C. *J. Catal.* **2013**, *298*, 10−17.
(88) Ovesen, C.; Clausen, B.; Schiøtz, J.; Stoltze, P.; Topsøe, H.; Nørskov, J. *J. Catal.* **1997**, *168*, 133−142.

DOI: 10.1021/acscatal.5b00442
ACS Catal. 2015, 5, 4201−4218

(89) Peter, M.; Fichtl, M. B.; Ruland, H.; Kaluza, S.; Muhler, M.; Hinrichsen, O. *Chem. Eng. J. (Amsterdam, Neth.)* **2012**, *203*, 480−491.
(90) Wöll, C. *Prog. Surf. Sci.* **2007**, *82*, 55−120.
(91) Kunat, M.; Meyer, B.; Traeger, F.; Wöll, C. *Phys. Chem. Chem. Phys.* **2006**, *8*, 1499−1504.
(92) Wang, J.; Hokkanen, B.; Burghaus, U. *Surf. Sci.* **2005**, *577*, 158−166.
(93) Wang, Y.; Xia, X.; Urban, A.; Qiu, H.; Strunk, J.; Meyer, B.; Muhler, M.; Wöll, C. *Angew. Chem., Int. Ed.* **2007**, *46*, 7315−7318.
(94) Wang, Y.; Kováčik, R.; Meyer, B.; Kotsis, K.; Stodt, D.; Staemmler, V.; Qiu, H.; Traeger, F.; Langenberg, D.; Muhler, M.; Wöll, C. *Angew. Chem., Int. Ed.* **2007**, *46*, 5624−5627.
(95) Kotsis, K.; Stodt, D.; Staemmler, V.; Kováčik, R.; Meyer, B.; Traeger, F.; Langenberg, D.; Strunskus, T.; Kunat, M.; Wöll, C. *Z. Phys. Chem.* **2008**, *222*, 891−915.
(96) Kurtz, M.; Strunk, J.; Hinrichsen, O.; Muhler, M.; Fink, K.; Meyer, B.; Wöll, C. *Angew. Chem., Int. Ed.* **2005**, *44*, 2790−2794.
(97) Polarz, S.; Strunk, J.; Ischenko, V.; van den Berg, M. W. E.; Hinrichsen, O.; Muhler, M.; Driess, M. *Angew. Chem., Int. Ed.* **2006**, *45*, 2965−2969.
(98) Kováčik, R.; Meyer, B.; Marx, D. *Angew. Chem., Int. Ed.* **2007**, *46*, 4894−4897.
(99) Kiss, J.; Witt, A.; Meyer, B.; Marx, D. *J. Chem. Phys.* **2009**, *130*, 184706.
(100) Meyer, B.; Marx, D.; Dulub, O.; Diebold, U.; Kunat, M.; Langenberg, D.; Wöll, C. *Angew. Chem., Int. Ed.* **2004**, *43*, 6641−6645.
(101) Dulub, O.; Meyer, B.; Diebold, U. *Phys. Rev. Lett.* **2005**, *95*, 136101.
(102) Meyer, B.; Rabaa, H.; Marx, D. *Phys. Chem. Chem. Phys.* **2006**, *8*, 1513−1520.
(103) Meyer, B. *Phys. Rev. B: Condens. Matter Mater. Phys.* **2004**, *69*, 045416.
(104) Wang, Y.; Meyer, B.; Yin, X.; Kunat, M.; Langenberg, D.; Traeger, F.; Birkner, A.; Wöll, C. *Phys. Rev. Lett.* **2005**, *95*, 266104.
(105) Qiu, H.; Meyer, B.; Wang, Y.; Wöll, Ch. *Phys. Rev. Lett.* **2008**, *101*, 236401.
(106) Fink, K. *Phys. Chem. Chem. Phys.* **2006**, *8*, 1482−1489.
(107) Rossmueller, G.; Kleinschmidt, V.; Kossmann, J.; Haettig, C. *J. Phys. Chem. C* **2009**, *113*, 1418−1425.
(108) Kossmann, J.; Rossmüller, G.; Hättig, C. *J. Chem. Phys.* **2012**, *136*, 034706.
(109) Kiss, J.; Frenzel, J.; Meyer, B.; Marx, D. *J. Chem. Phys.* **2013**, *139*, 044705.
(110) Rasmussen, D. B.; Janssens, T. V.; Temel, B.; Bligaard, T.; Hinnemann, B.; Helveg, S.; Sehested, J. *J. Catal.* **2012**, *293*, 205−214.
(111) Marx, D.; Hutter, J. *Ab Initio Molecular Dynamics: Basic Theory and Advanced Methods*; Cambridge University Press: Cambridge, U. K., 2009.
(112) Tohji, K.; Udagawa, Y.; Mizushima, T.; Ueno, A. *J. Phys. Chem.* **1985**, *89*, 5671−5676.
(113) Campbell, C. T.; Daube, K. A.; White, J. *Surf. Sci.* **1987**, *182*, 458−476.
(114) Zhang, R.; Ludviksson, A.; Campbell, C. *Catal. Lett.* **1994**, *25*, 277−292.
(115) Kiss, J.; Frenzel, J.; Nair, N. N.; Meyer, B.; Marx, D. *J. Chem. Phys.* **2011**, *134*, 064710.
(116) Frenzel, J.; Kiss, J.; Nair, N. N.; Meyer, B.; Marx, D. *Phys. Status Solidi B* **2013**, *250*, 1174−1190.
(117) Frenzel, J.; Marx, D. *J. Chem. Phys.* **2014**, *141*, 124710.
(118) Meyer, B.; Marx, D. *Phys. Rev. B: Condens. Matter Mater. Phys.* **2004**, *69*, 235420.
(119) Meyer, B.; Marx, D. *Phys. Rev. B: Condens. Matter Mater. Phys.* **2003**, *67*, 035403.
(120) Yudanov, I. V.; Genest, A.; Schauermann, S.; Freund, H.-J.; Rösch, N. *Nano Lett.* **2012**, *12*, 2134−2139.
(121) Raybaud, P.; Chizallet, C.; Mager-Maury, C.; Digne, M.; Toulhoat, H.; Sautet, P. *J. Catal.* **2013**, *308*, 328−340.
(122) Ammal, S. C.; Heyden, A. *ACS Catal.* **2014**, *4*, 3654−3662.
(123) Vilhelmsen, L. B.; Hammer, B. *ACS Catal.* **2014**, *4*, 1626−1631.
(124) Olmos-Asar, J. A.; Monachino, E.; Dri, C.; Peronio, A.; Africh, C.; Lacovig, P.; Comelli, G.; Baldereschi, A.; Peressi, M.; Vesselli, E. *ACS Catal.* **2015**, *5*, 2719−2726.
(125) Lang, S. M.; Fleischer, I.; Bernhardt, T. M.; Barnett, R. N.; Landman, U. *ACS Catal.* **2015**, *5*, 2275−2289.
(126) Yoon, B.; Häkkinen, H.; Landman, U.; Wörz, A. S.; Antonietti, J.-M.; Abbet, S.; Judai, K.; Heiz, U. *Science* **2005**, *307*, 403−407.
(127) Röttgen, M. A.; Abbet, S.; Judai, K.; Antonietti, J.-M.; Wörz, A. S.; Arenz, M.; Henry, C. R.; Heiz, U. *J. Am. Chem. Soc.* **2007**, *129*, 9635−9639.
(128) Rodriguez, J.; Liu, P.; Viñes, F.; Illas, F.; Takahashi, Y.; Nakamura, K. *Angew. Chem., Int. Ed.* **2008**, *47*, 6685−6689.
(129) Herzing, A. A.; Kiely, C. J.; Carley, A. F.; Landon, P.; Hutchings, G. J. *Science* **2008**, *321*, 1331−1335.
(130) Lei, Y.; Mehmood, F.; Lee, S.; Greeley, J.; Lee, B.; Seifert, S.; Winans, R. E.; Elam, J. W.; Meyer, R. J.; Redfern, P. C.; Teschner, D.; Schlögl, R.; Pellin, M. J.; Curtiss, L. A.; Vajda, S. *Science* **2010**, *328*, 224−228.
(131) Bruix, A.; Rodriguez, J. A.; Ramírez, P. J.; Senanayake, S. D.; Evans, J.; Park, J. B.; Stacchiola, D.; Liu, P.; Hrbek, J.; Illas, F. *J. Am. Chem. Soc.* **2012**, *134*, 8968−8974.
(132) Schweinberger, F. F.; Berr, M. J.; Döblinger, M.; Wolff, C.; Sanwald, K. E.; Crampton, A. S.; Ridge, C. J.; Jäckel, F.; Feldmann, J.; Tschurl, M.; Heiz, U. *J. Am. Chem. Soc.* **2013**, *135*, 13262−13265.
(133) Perdew, J. P.; Burke, K.; Ernzerhof, M. *Phys. Rev. Lett.* **1996**, *77*, 3865−3868.
(134) Perdew, J. P.; Burke, K.; Ernzerhof, M. *Phys. Rev. Lett.* **1997**, *78*, 1396.
(135) Vanderbilt, D. *Phys. Rev. B: Condens. Matter Mater. Phys.* **1990**, *41*, 7892−7895.
(136) Giannozzi, P.; Baroni, S.; Bonini, N.; Calandra, M.; Car, R.; Cavazzoni, C.; Ceresoli, D.; Chiarotti, G. L.; Cococcioni, M.; Dabo, I.; Dal Corso, A.; de Gironcoli, S.; Fabris, S.; Fratesi, G.; Gebauer, R.; Gerstmann, U.; Gougoussis, C.; Kokalj, A.; Lazzeri, M.; Martin-Samos, L.; Marzari, N.; Mauri, F.; Mazzarello, R.; Paolini, S.; Pasquarello, A.; Paulatto, L.; Sbraccia, C.; Scandolo, S.; Sclauzero, G.; Seitsonen, A. P.; Smogunov, A.; Umari, P.; Wentzcovitch, R. M. *J. Phys.−Condens. Mater.* **1976**, *13*, 5188−5192.
(137) Monkhorst, H. J.; Pack, J. D. *Phys. Rev. B* **1976**, *13*, 5188−5192.
(138) Löwdin, P.-O. *Adv. Quantum Chem.* **1970**, *5*, 185−199.
(139) Farnesi Camellone, M.; Marx, D. *J. Phys. Chem. Lett.* **2013**, *4*, 514−518.
(140) Schwabe, T.; Grimme, S. *Phys. Chem. Chem. Phys.* **2007**, *9*, 3397−3406.
(141) Farnesi Camellone, M.; Marx, D. *J. Phys. Chem. C* **2014**, *118*, 20989−21000.
(142) Car, R.; Parrinello, M. *Phys. Rev. Lett.* **1985**, *55*, 2471−2474.
(143) CPMD. http://www.cpmd.org/. (Accessed 3/21/2012) Copyright IBM Corp 1990−2008, Copyright MPI für Festkörperforschung Stuttgart 1997−2001.
(144) Martyna, G. J.; Klein, M. L.; Tuckerman, M. *J. Chem. Phys.* **1992**, *97*, 2635−2643.
(145) Laio, A.; Parrinello, M. *Proc. Natl. Acad. Sci. U. S. A.* **2002**, *99*, 12562−12566.
(146) Laio, A.; Gervasio, F. L. *Rep. Prog. Phys.* **2008**, *71*, 126601.
(147) Iannuzzi, M.; Laio, A.; Parrinello, M. *Phys. Rev. Lett.* **2003**, *90*, 238302.
(148) Laio, A.; Parrinello, M. *Computer Simulations in Condensed Matter: Computing Free Energies and Accelerating Rare Events with Metadynamics*; Springer Verlag: Berlin, 2006; Vol. *703*; pp 315−347.
(149) Ensing, B.; Laio, A.; Parrinello, M.; Klein, M. L. *J. Phys. Chem. B* **2005**, *109*, 6676−6687.
(150) Bussi, G.; Laio, A.; Parrinello, M. *Phys. Rev. Lett.* **2006**, *96*, 090601.
(151) Raiteri, P.; Laio, A.; Gervasio, F. L.; Micheletti, C.; Parrinello, M. *J. Phys. Chem. B* **2006**, *110*, 3533−3539.

DOI: 10.1021/acscatal.5b00442
ACS Catal. 2015, 5, 4201−4218

(152) Madon, R. J.; Braden, D.; Kandoi, S.; Nagel, P.; Mavrikakis, M.; Dumesic, J. A. *J. Catal.* **2011**, *281*, 1−11.
(153) Rodriguez, J. A.; Hanson, J. C.; Stacchiola, D.; Senanayake, S. D. *Phys. Chem. Chem. Phys.* **2013**, *15*, 12004−12025.
(154) Rodriguez, J. A.; Liu, P.; Hrbek, J.; Evans, J.; Pérez, M. *Angew. Chem., Int. Ed.* **2007**, *46*, 1329−1332.
(155) Jones, P. M.; May, J. A.; Reitz, J. B.; Solomon, E. I. *Inorg. Chem.* **2004**, *43*, 3349−3370.
(156) Kolasinski, K. W. *Surf. Sci.: Foundations of Catalysis and Nanoscience*; Wiley: New York, 2008.
(157) Sanchez, A.; Abbet, S.; Heiz, U.; Schneider, W.-D.; Häkkinen, H.; Barnett, R. N.; Landman, U. *J. Phys. Chem. A* **1999**, *103*, 9573−9578.
(158) Artrith, N.; Hiller, B.; Behler, J. *Phys. Status Solidi B* **2013**, *250*, 1191−1203.
(159) Valden, M.; Lai, X.; Goodman, D. W. *Science* **1998**, *281*, 1647−1650.
(160) Fu, Q.; Saltsburg, H.; Flytzani-Stephanopoulos, M. *Science* **2003**, *301*, 935−938.
(161) Parkinson, G. S.; Novotny, Z.; Argentero, G.; Schmid, M.; Pavelec, J.; Kosak, R.; Blaha, P.; Diebold, U. *Nat. Mater.* **2013**, *12*, 724−728.
(162) Rasmussen, P.; Holmblad, P.; Askgaard, T.; Ovesen, C.; Stoltze, P.; Nørskov, J.; Chorkendorff, I. *Catal. Lett.* **1994**, *26*, 373−381.
(163) Schreiner, E.; Nair, N. N.; Marx, D. *J. Am. Chem. Soc.* **2008**, *130*, 2768−2770.
(164) Nair, N. N.; Schreiner, E.; Marx, D. *J. Am. Chem. Soc.* **2008**, *130*, 14148−14160.
(165) Schreiner, E.; Nair, N. N.; Marx, D. *J. Am. Chem. Soc.* **2009**, *131*, 13668−13675.
(166) Schreiner, E.; Nair, N. N.; Wittekindt, C.; Marx, D. *J. Am. Chem. Soc.* **2011**, *133*, 8216−8226.
(167) Muñoz-Santiburcio, D.; Wittekindt, C.; Marx, D. *Nat. Commun.* **2013**, *4*, 2349.

DOI: 10.1021/acscatal.5b00442
ACS Catal. 2015, 5, 4201−4218